Physics of Extreme Massive Stars

Marie-Curie-RISE project funded by the European Union

Determination of Fundamental Parameters of Massive Stars

Lydia Cidale

Facultad de Ciencias Astronómicas y Geofísicas
National University of La Plata (UNLP)
Instituto de Astrofísica - CONICET-UNLP
Argentina

FCAG·UNLP

IALP CONICET UNLP

Río de Janeiro, June 24-28, 2024

For a complete description of a star, the following set of parameters is essential

- Mass,
- Luminosity,
- Radius,
- Age,
- Pulsation period,

For a complete description of a star, the following set of parameters is essential

- Mass,
- Luminosity,
- Radius,
- Age,
- Pulsation period,
- Chemical composition,
- Angular momentum,
- Magnetic field,
- Mass-loss rate,
- Circumstellar environment (CE).

For a complete description of a star, the following set of parameters is essential

- Mass,
- Luminosity,
- Radius,
- Age,
- Pulsation period,

- Chemical composition,
- Angular momentum,
- Magnetic field,
- Mass-loss rate,
- Circumstellar environment (CE).

The determination of several of these parameters requires a **high-spectral resolution**.
Most of them are integrated values and other vary across the disk, the CE or the evolution phase.

Independent set of parameters are R_*, M_* and L_*

Dependent set of parameters T_{eff}, log g, and ρ_m

$L_* = 4 \pi R_*^2 \sigma T_{eff}^4$

$g = GM_*/R_*^2$

$\rho_m = 3M_*/4\pi R_*^3$

$P^2 = G \rho_m$

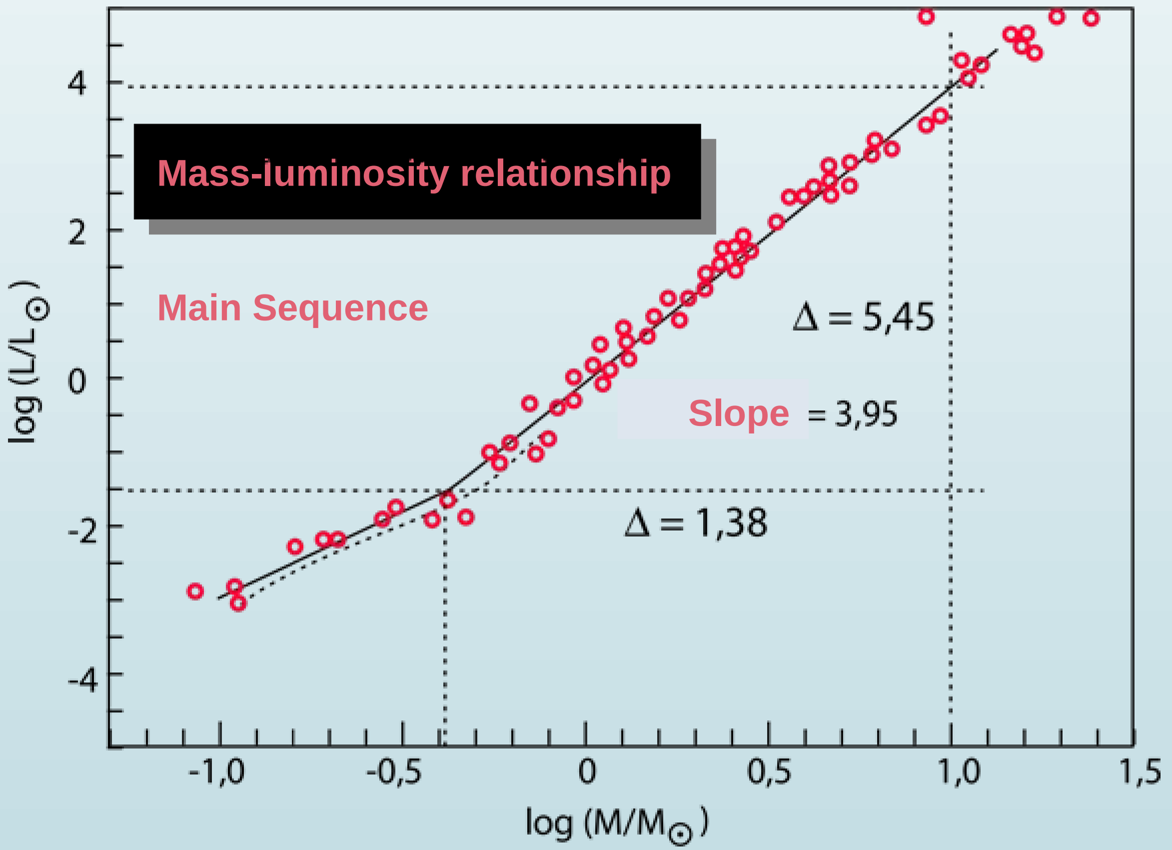

Motivations

- To test models of stellar evolution and stellar atmospheres.
- To precise the evolutionary phases.
- To improve our understanding on stellar pulsations, and rotation in massive stars.

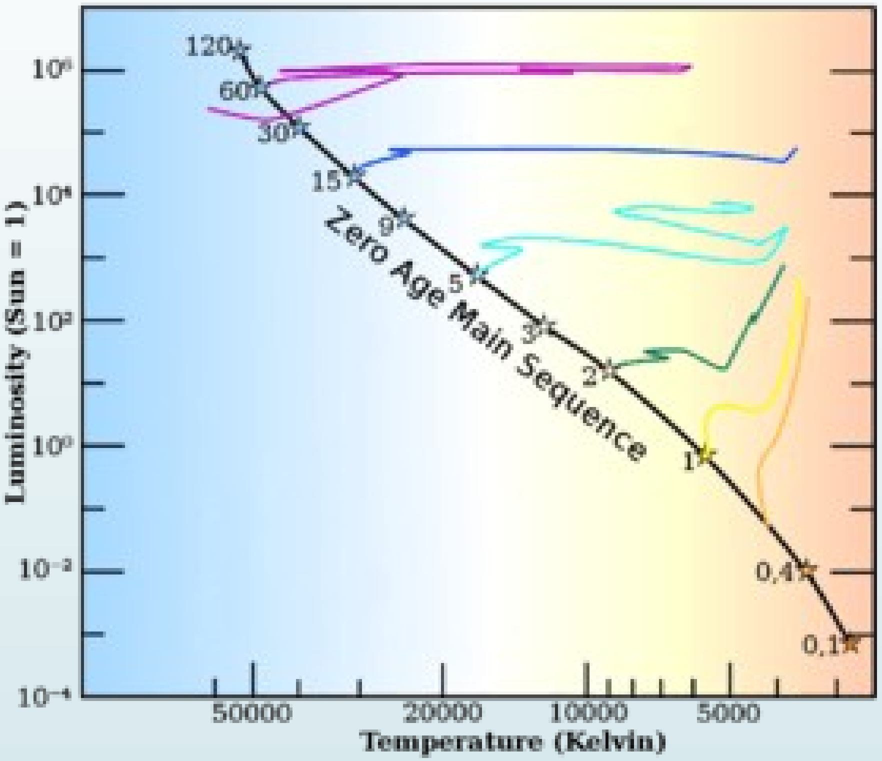

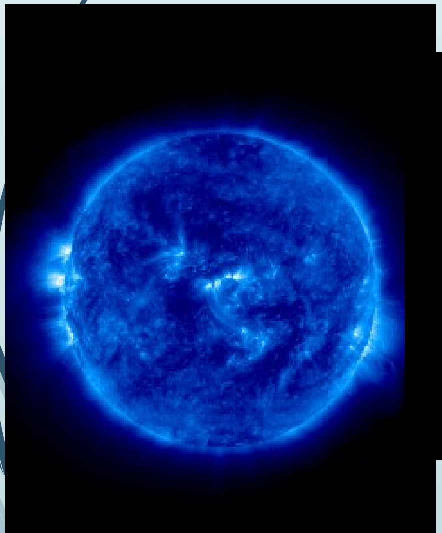

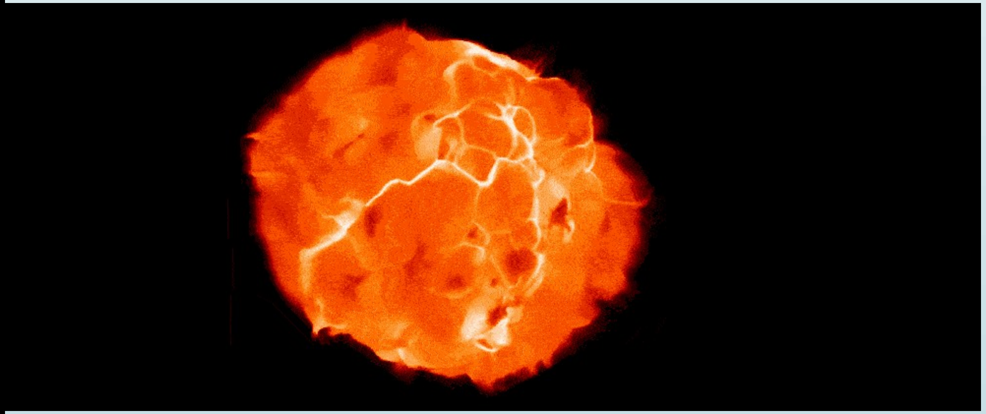

Motivations

- To compute synthetic spectra

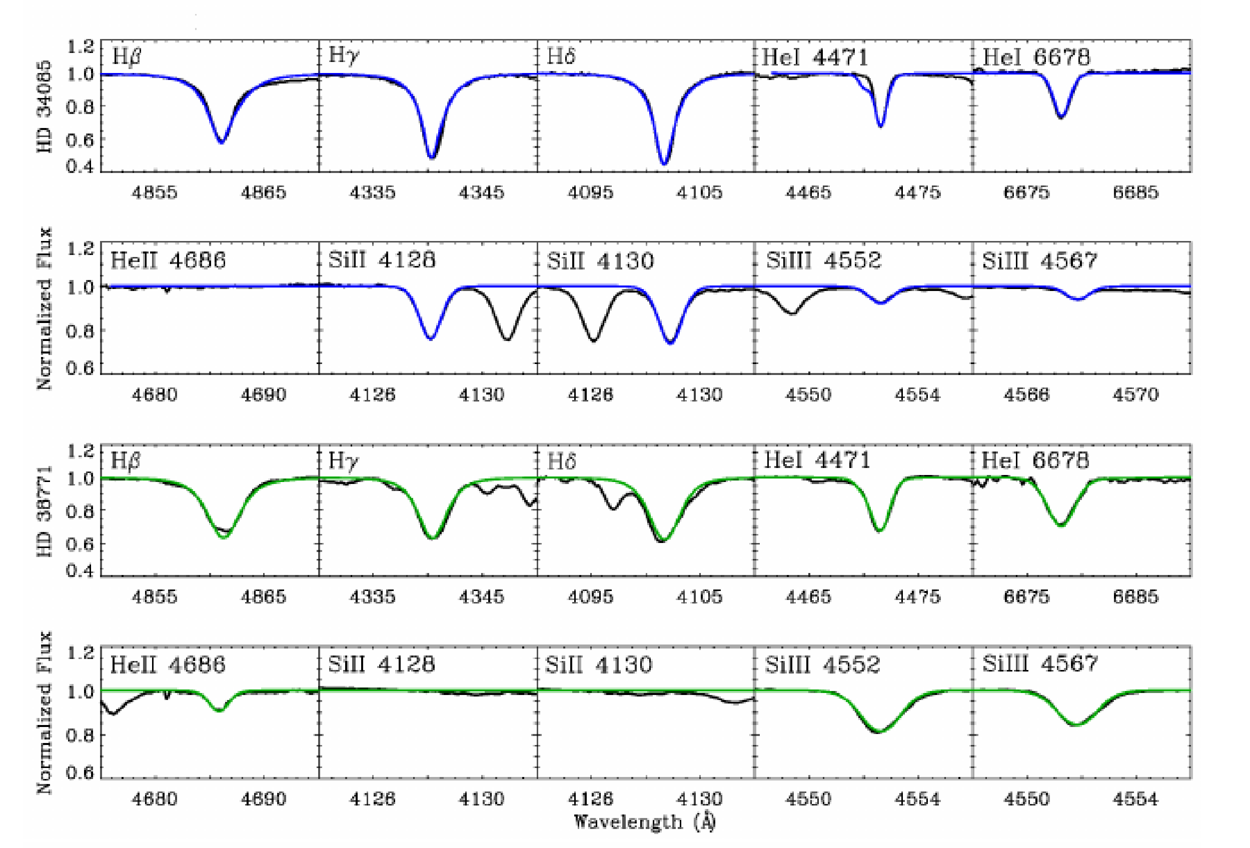

Motivations

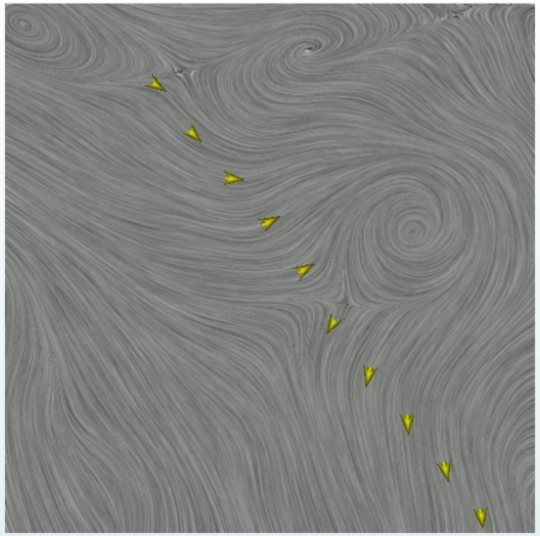

- To compute synthetic spectra
- To calculate the wind hydrodynamics and mass-loss rates.

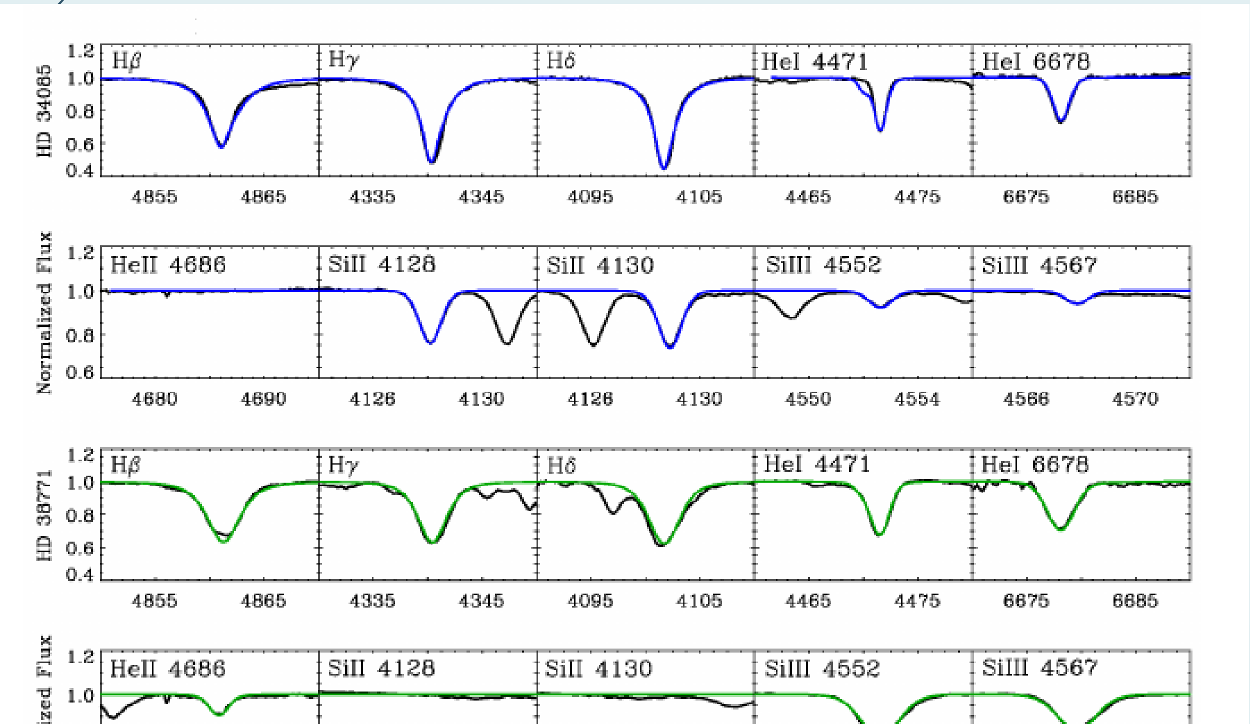

Motivations

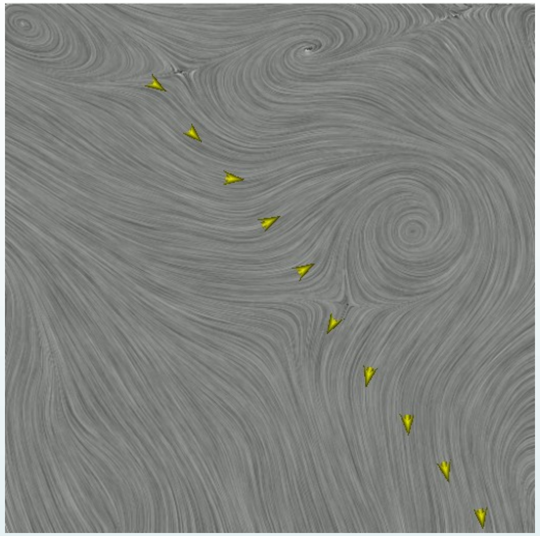

- To compute synthetic spectra
- To calculate the wind hydrodynamics and mass-loss rates.
- To analyse and discuss distances and the Wind-Momentum luminosity relationship.

$$D_{\rm mom} = \dot{M}\, v_\infty\, R^{0.5} \propto L^{1/\alpha_{\rm eff}},$$

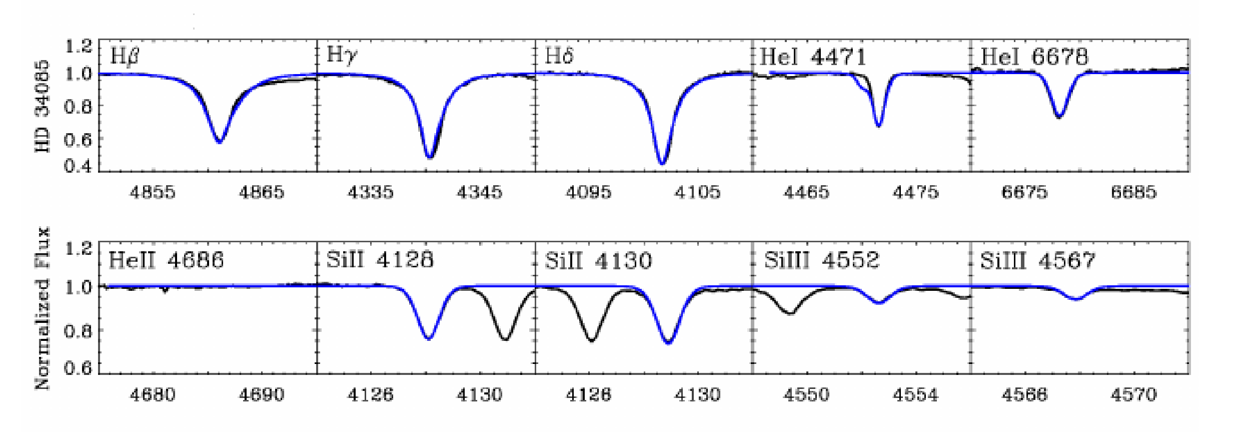

Motivations

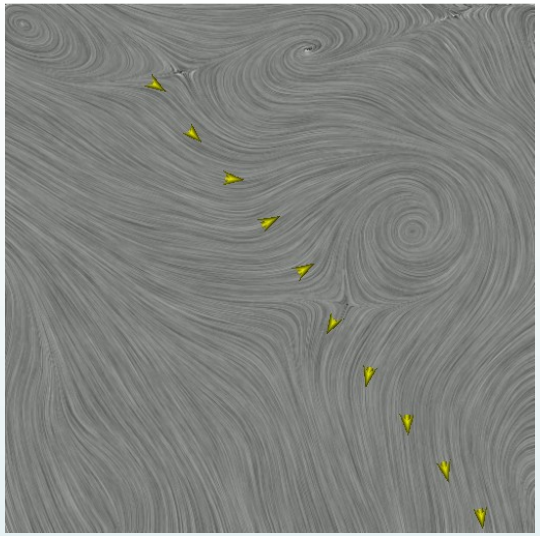

- To compute synthetic spectra
- To calculate the wind hydrodynamics and mass-loss rates.
- To analyse and discuss distances and the Wind-Momentum luminosity relationship.

To derive stellar parameter of peculiar (emission line) stars: such as Be and B[e].

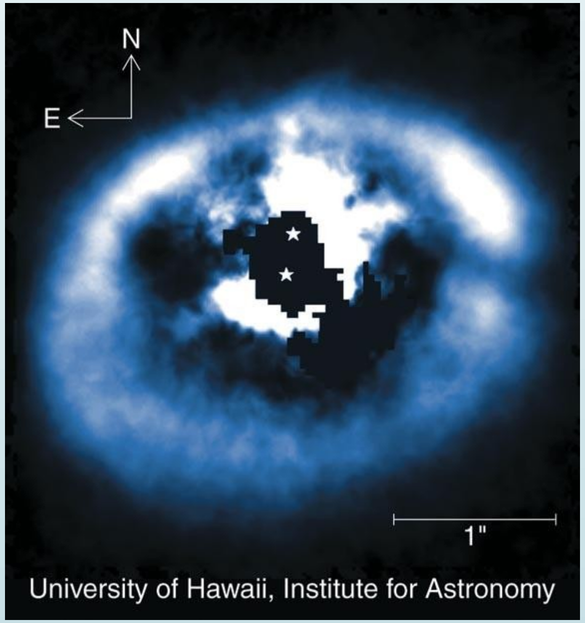

$$D_{\mathrm{mom}} = \dot{M}\, v_{\infty}\, R^{0.5} \propto L^{1/\alpha_{\mathrm{eff}}},$$

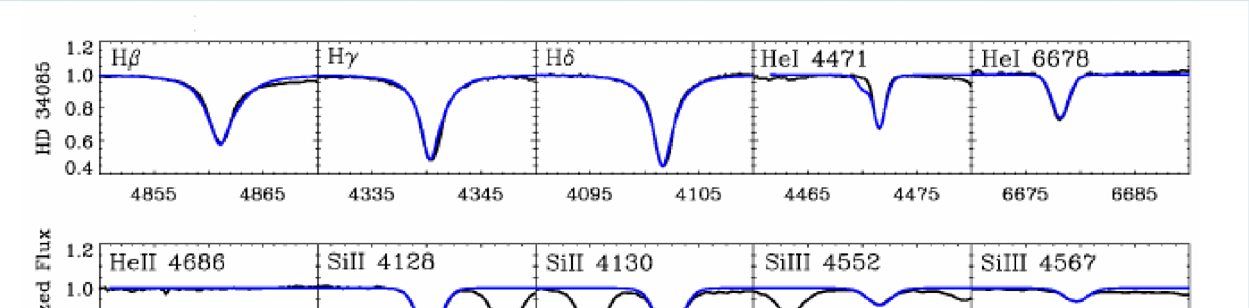

R_* is the **most critical** value and **sensitive** to distance

-

R_* is the most critical value and sensitive to distance

- Eclipsing binaries

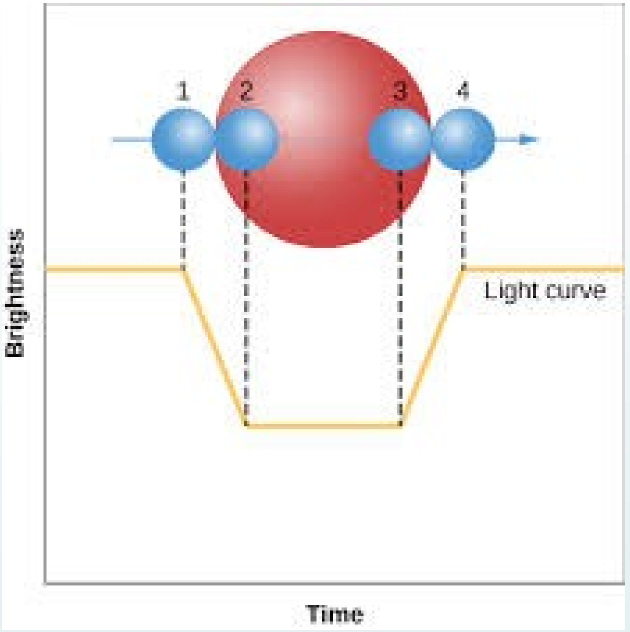

R_* is the most critical value and sensitive to distance

- **Eclipsing binaries**
- **Lunar ocultation**

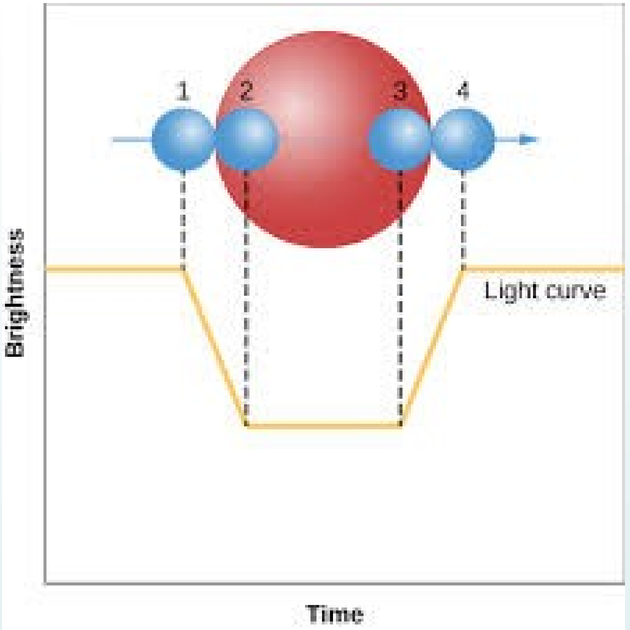

R_* is the **most critical** value and **sensitive** to distance

- **Eclipsing binaries**
- **Lunar ocultation**
- **Interferometry**

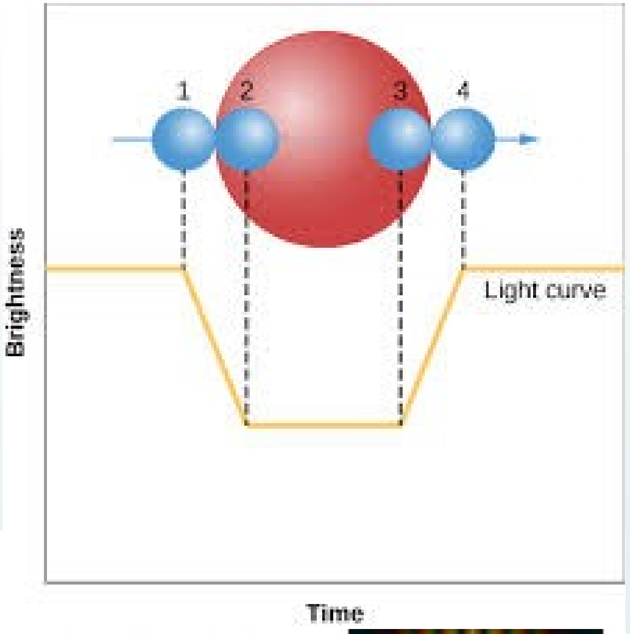

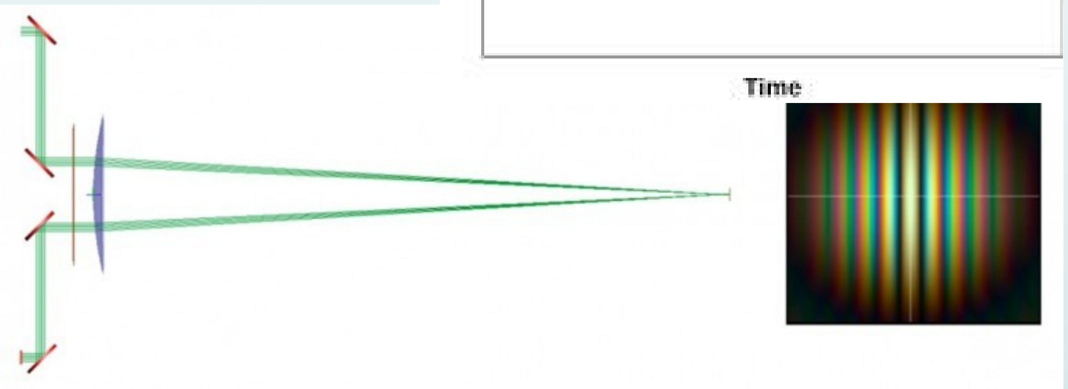

R* is the **most critical** value and **sensitive** to distance

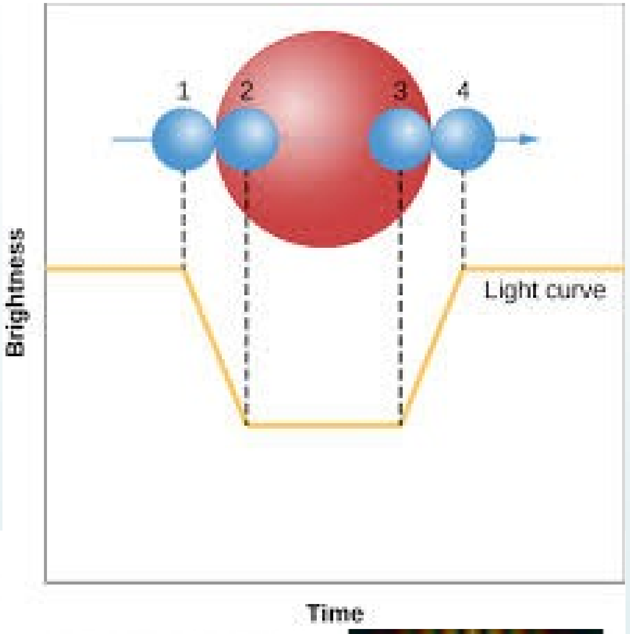

- Eclipsing binaries
- Lunar ocultation
- Interferometry
- Photometry

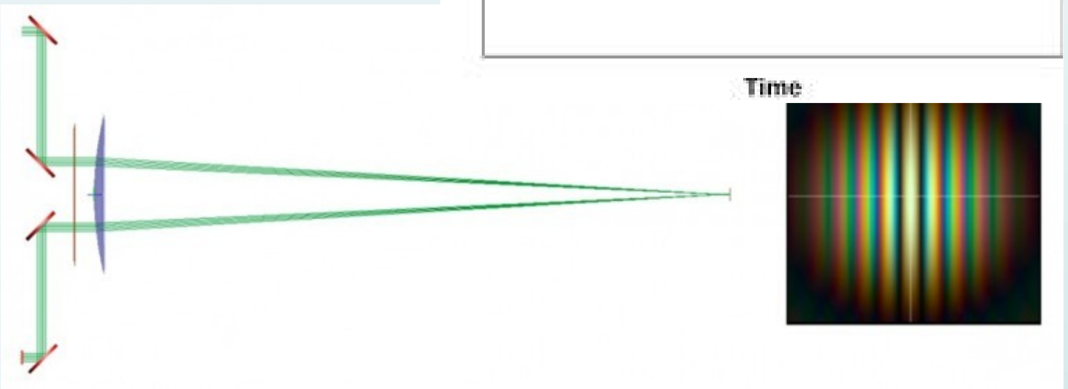

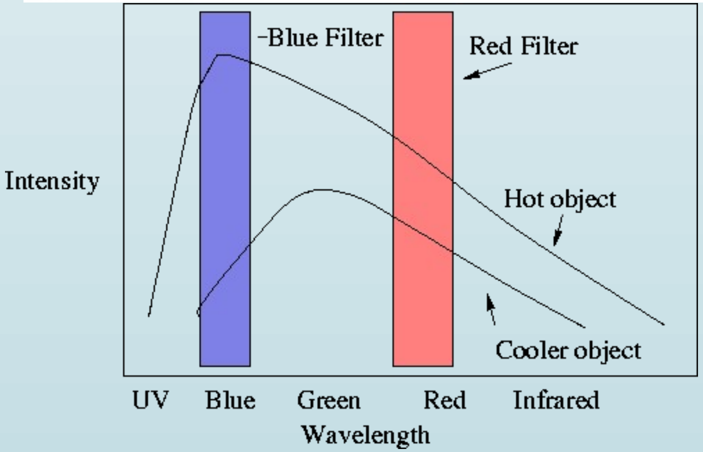

Interferometric measurements can also derive asymmetric shapes of stellar surfaces if baselines of different orientation are used.

First detection of an oblate photosphere of the fast rotator Altair (Van Belle, 2001)

VLTI measurements of the asymmetric shape of the rotating Be star Achernar (Domiciano de Souza et al., 2003), which it is much flatter than theoretically expected (3/2 of the Roche model)

This particularity is explain by a shellular rotation regime, where the angular velocity is constant on level surfaces, but increases with depth (Zahn et al 2010, A&A 517, 7).

The differential shellular rotation was first invoked by Zorec et al. (2005)

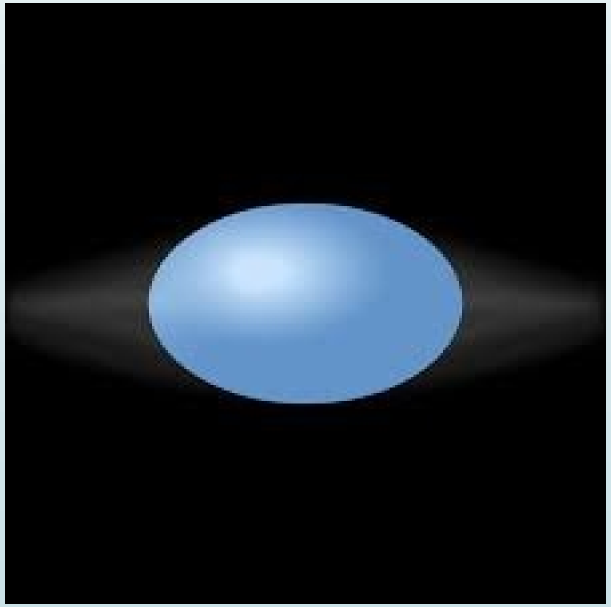

Determination of Stellar Parameters (Teff, log g and μ) Spectroscopic Analysis

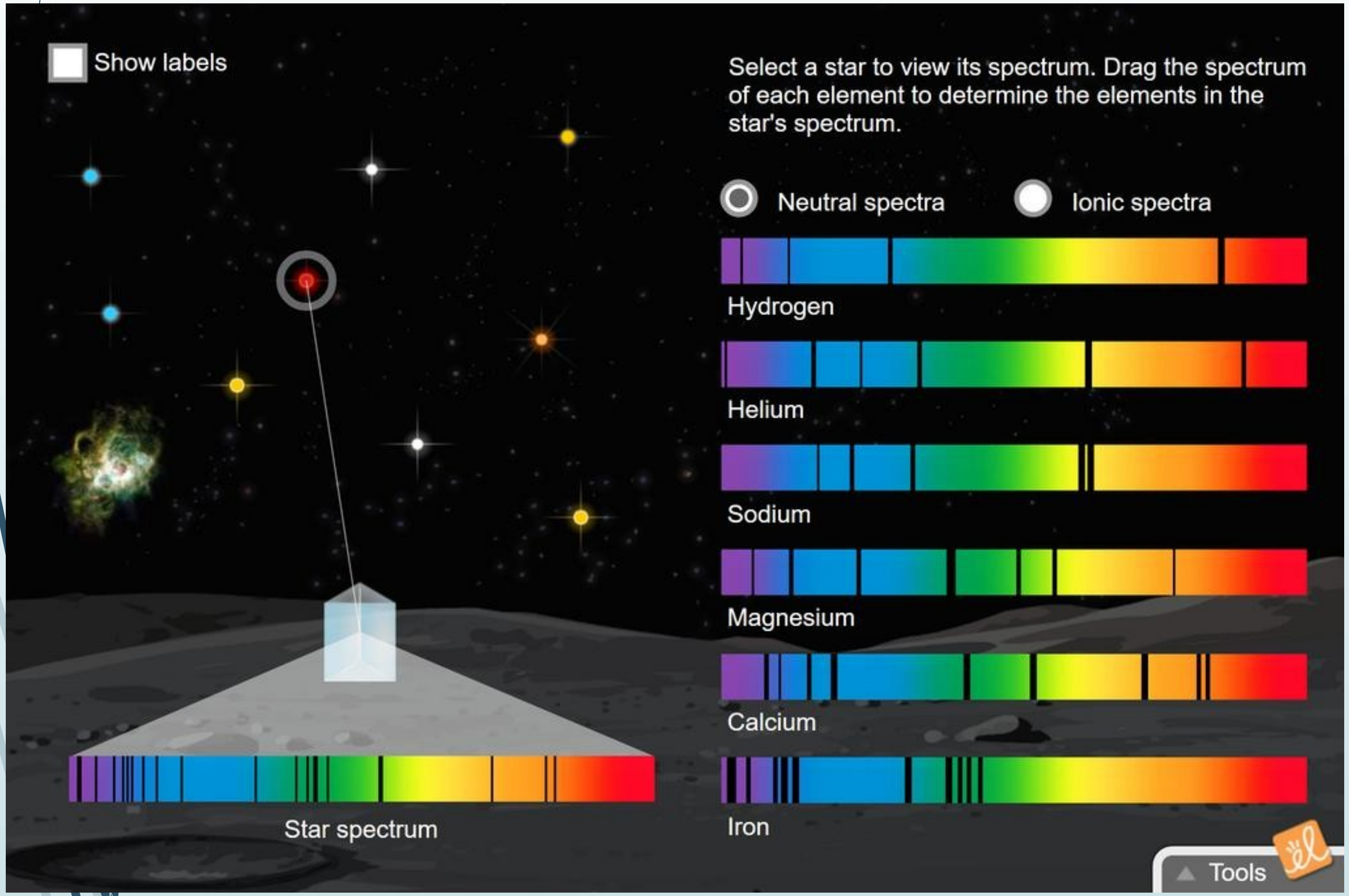

Gizmos - Star spectra

Line by line analysis (Ews & line strenghts)

Synthetic modelling and fitting with the observed spectrum

The BCD classification, based on the Balmer discontinuity

Atmospheric Models (plane parallel approximation)

- Kurucz (Kurucz et al., 1993)
- MARCS (Gustafsson et al., 2008)
- Tlusty (Lanz & Hubeny 1996) (Teff > 15000 K)
- ULySS (a set of models or an empirical library of objects, Koleva et al. 2009)

FGK solar-type stars
(LTE)
Line blanketing

OBA-type stars
(NLTE)
Line lanketing

Fittings are often based on precalculated grids of synthetic models

All the models depend on the He/H ratio

Stellar parameters

- **SED fittings → T_{eff} and log g**

Teff (effective temperature) is obtained from the **continuum flux.**

The fittings depend $(R^*/D)^2$, $A_V = R^*\ E(B-V)$

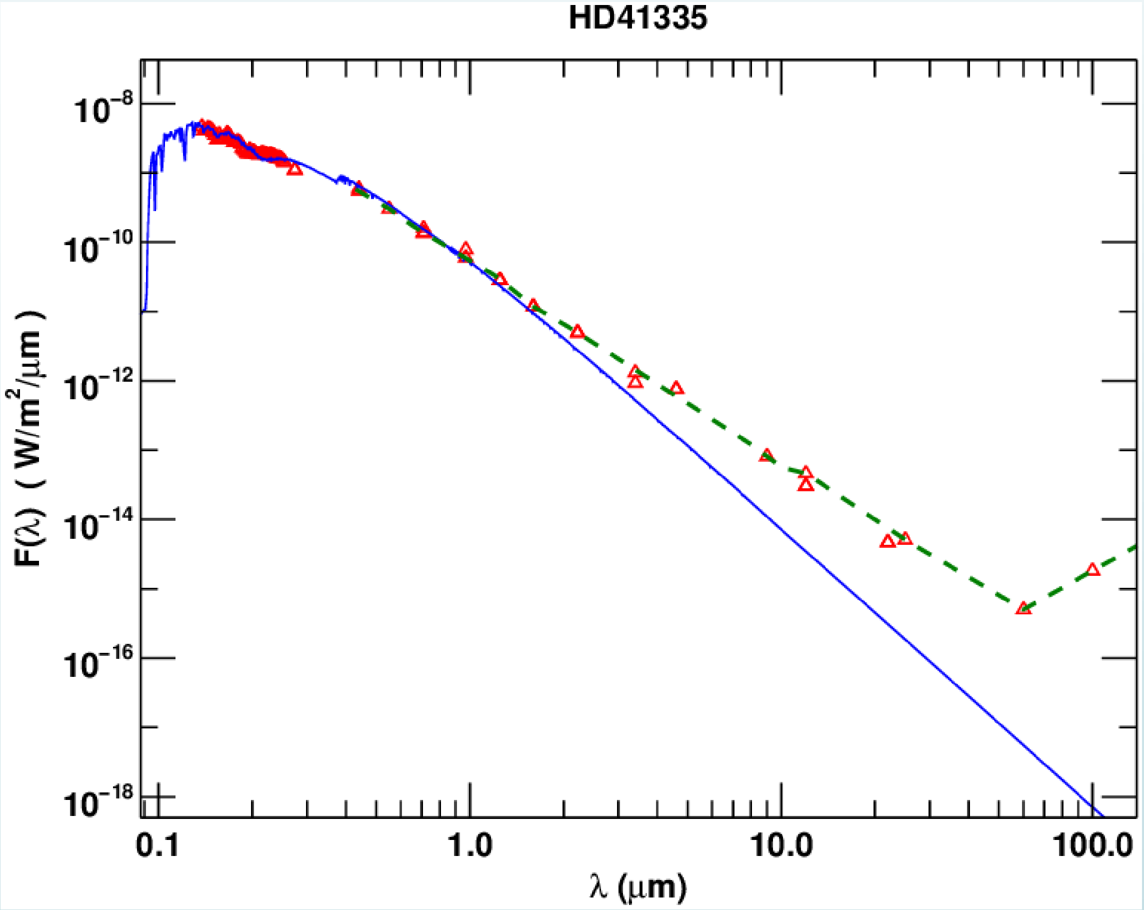

Based on line-blanketed LTE stellar atmospheres from Kurucz (1979)

$$F = \frac{f}{\pi}\left(\frac{d}{R}\right)^2 = \frac{4f}{\pi\theta^2}$$

$$\Theta = 0.1692 + 0.2828[u-b] - 0.0195[u-b]^2$$

$$\Theta = \frac{5040\,\mathrm{K}}{T_{\mathrm{eff}}}$$

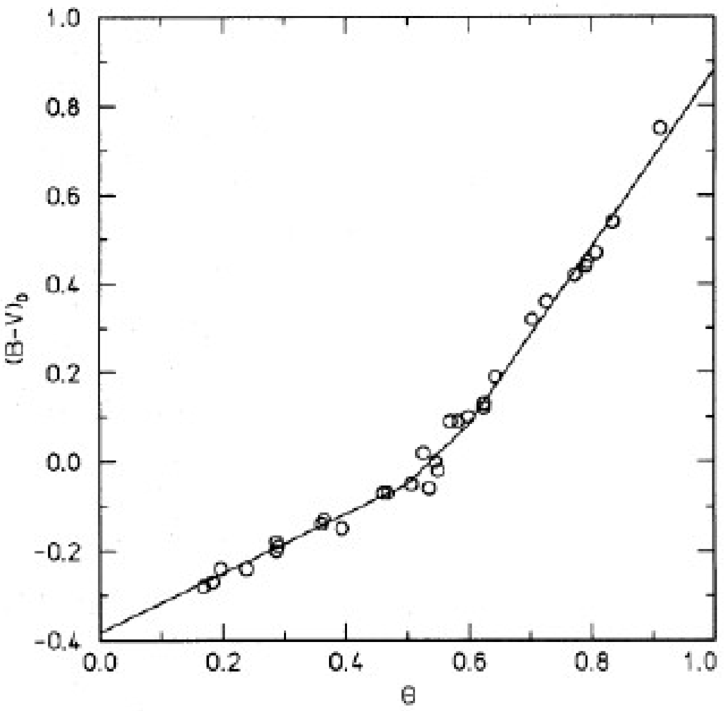

Fig. 8. $(B-V)_0$ calibration

Napiwotzki et al., 1993, A&A, 268, 653
Moon & Dworetsky, 1985, MNRAS, 217, 305

BCD Spectrophotometric Classification System

T_{eff}, log g, M_{bol}, M_v and A_v

Balmer Jump

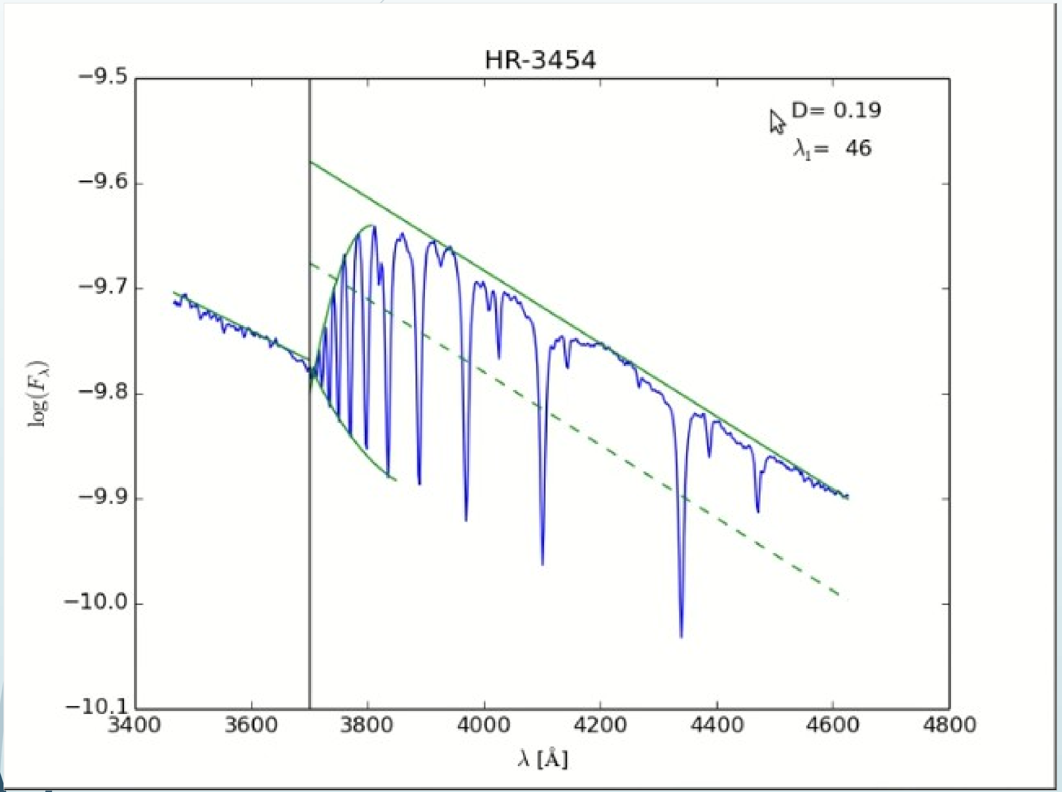

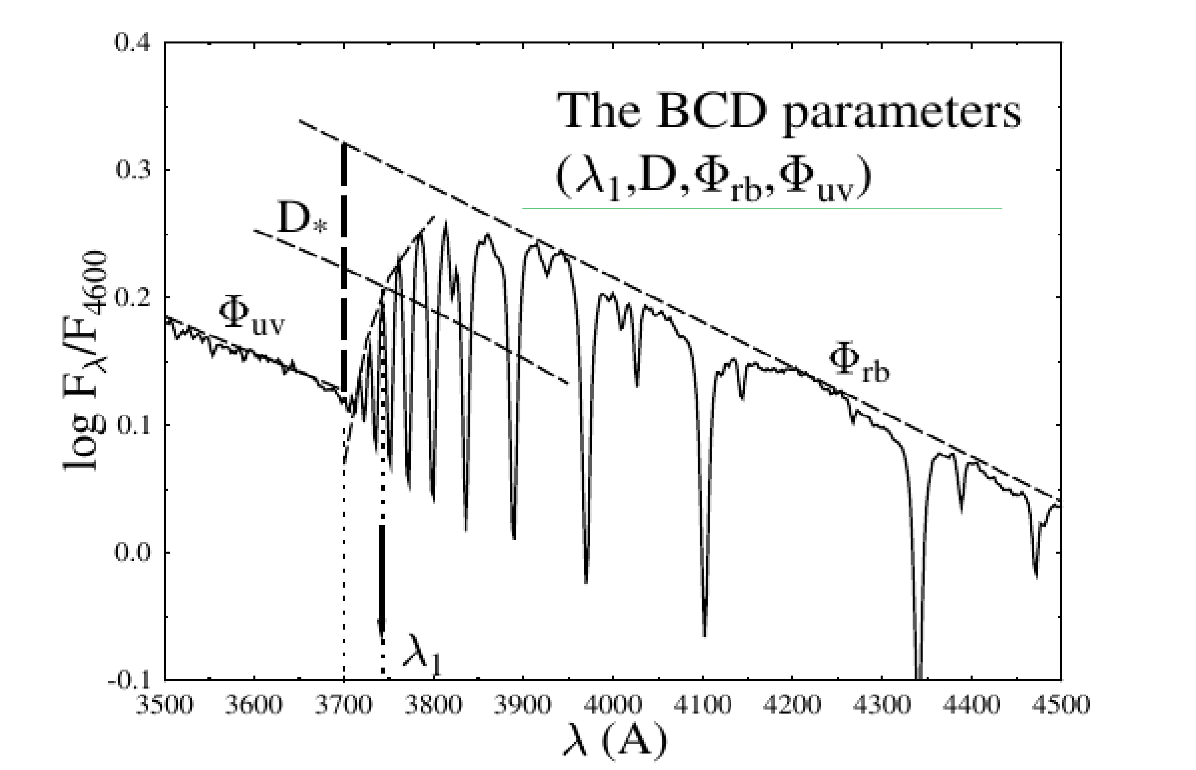

Fig. A.1. Graphical explanation of the BCD (λ_1, D, Φ_{rb}, Φ_{uv}) parameters.

Barbier, D., & Chalonge, D. 1941, Ann. Astrophys., 4, 30
Chalonge, D., & Divan, L. 1952, Ann. Astrophys., 15, 201
Chalonge, D., & Divan, L. 1973, A&A, 23, 69
Chalonge, D., & Divan, L. 1977, A&A, 55, 117

Barbier, Chalonge & Divan

BCD calibrations

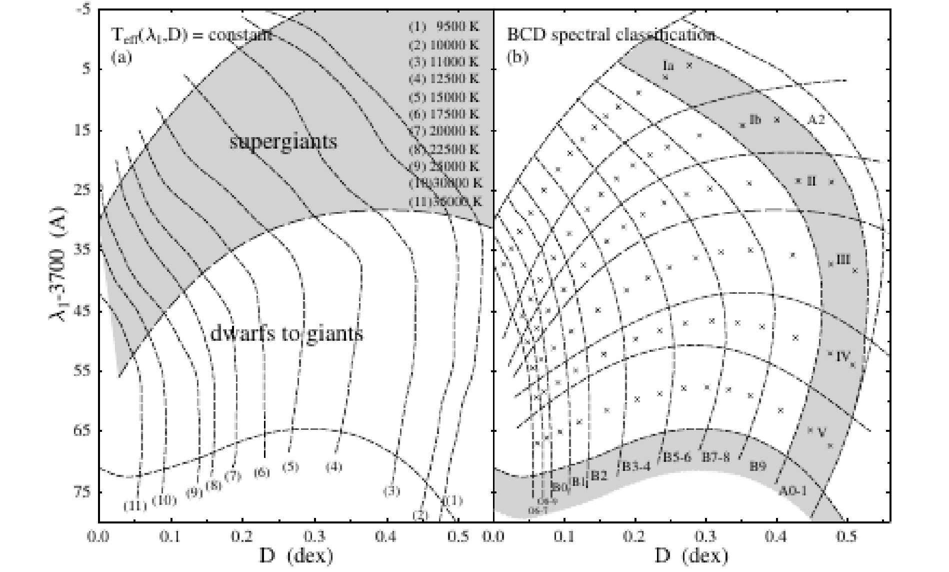

Fig. 10. **a)**: spline-smoothed $T_{eff}(\lambda_1, D)$ = const. curves for the values of effective temperature given in the box at right-top; **b)** the curvilinear-quadrilateral BCD (λ_1, D) spectral classification diagram, where the corresponding 2D MK spectral types (bottom shaded strip) and the luminosity classes (left shaded strip) are indicated. The cross-marks indicate the mid-point of each MK spectral type-luminosity class box where the $T_{eff}(\lambda_1, D)$ values given in Table 3 were obtained.

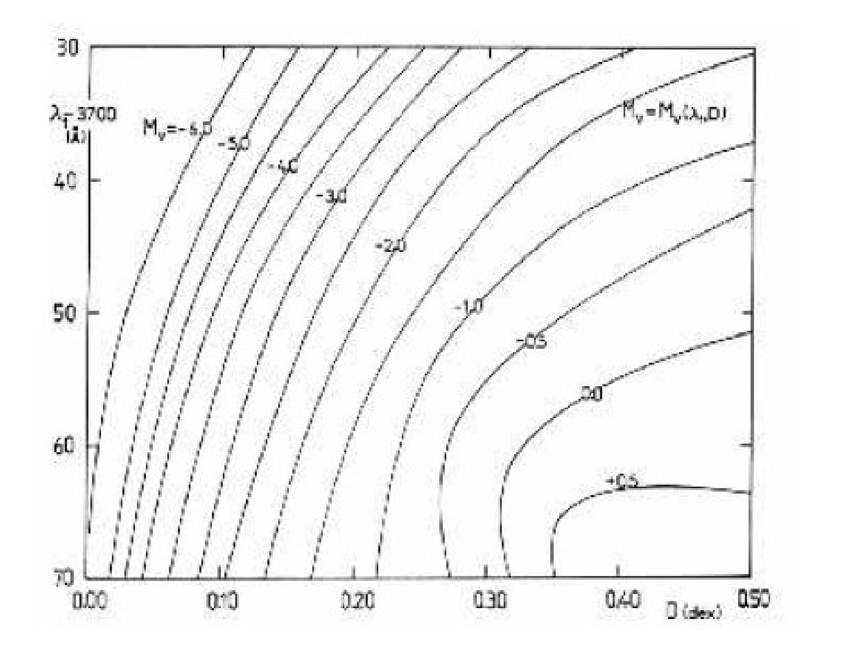

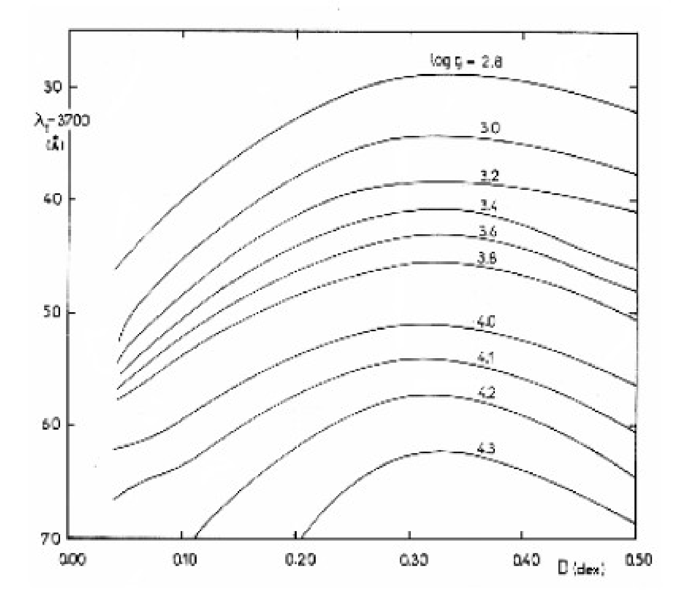

$$E(B-V)=0.68\left(\Phi_b-\Phi_b^0\right)=0.75\left(\Phi_{bb}-\Phi_{bb}^0\right)$$
$$A_V=2.11\left(\Phi_b-\Phi_b^0\right)=2.33\left(\Phi_{bb}-\Phi_{bb}^0\right)$$

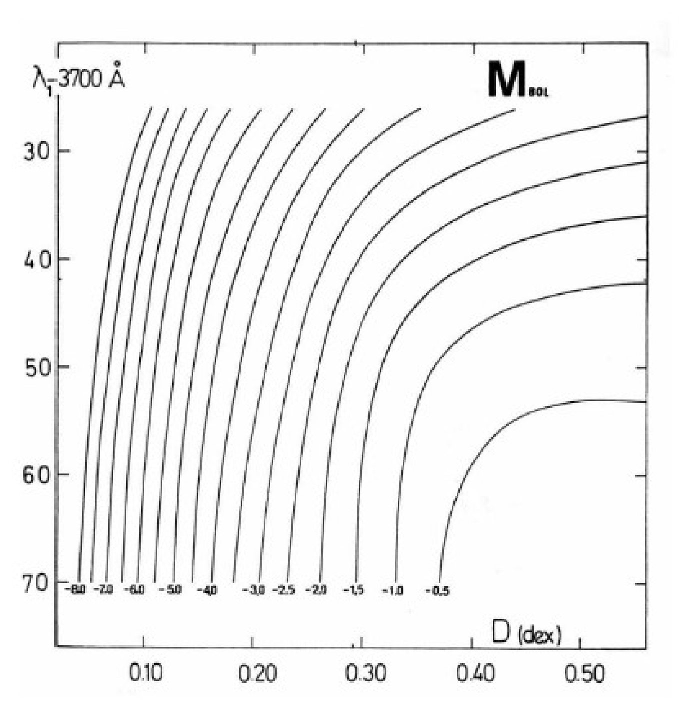

Zorec et al (2009), A&A 501,297
Zorec et al. (2023) Galaxies 11, 18

BCD T_{eff} vs. Line models

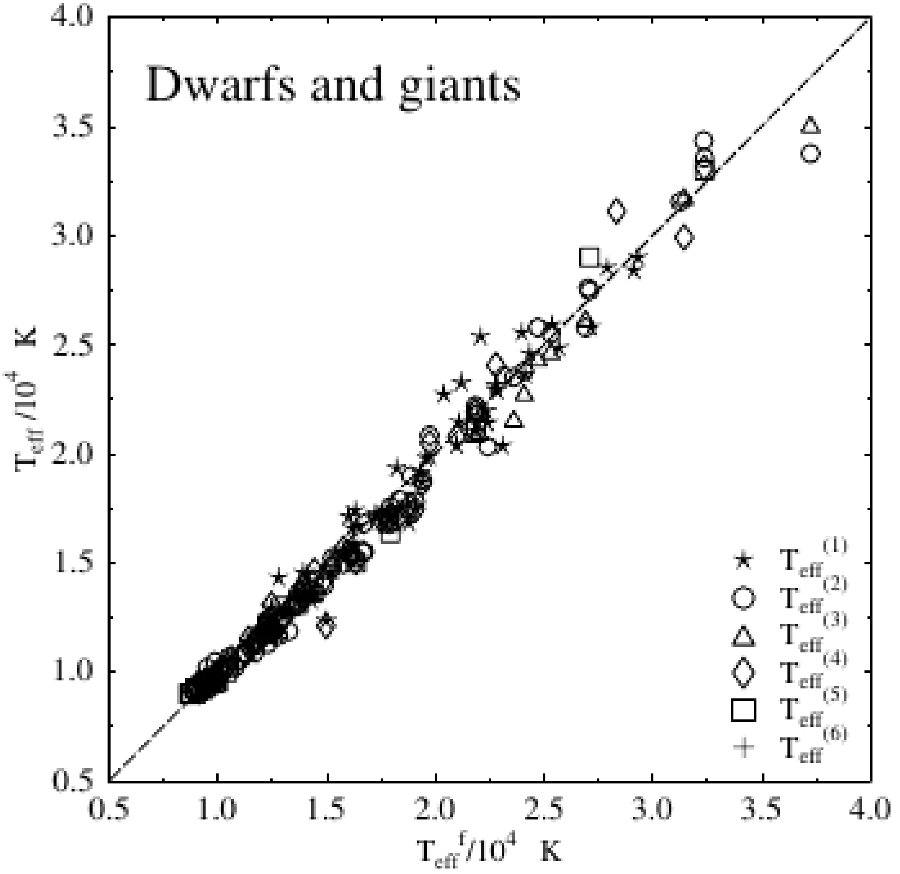

Fig. 6. Effective temperatures of dwarfs and giants determined by other authors (ordinates) against the $T^f_{\rm eff}$ estimates obtained in the present work (abscissa).

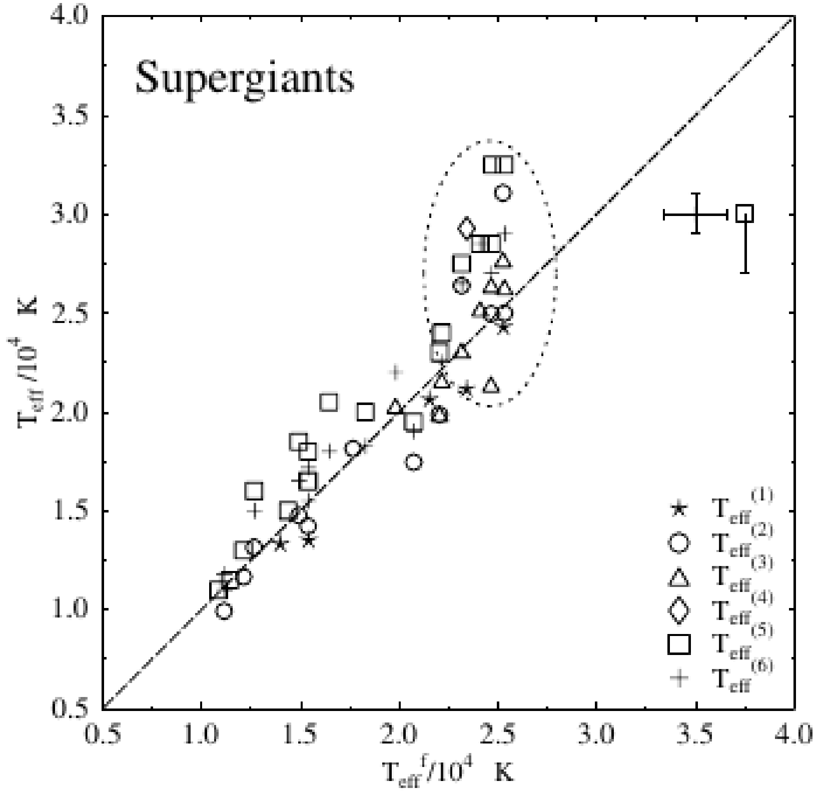

Fig. 7. Effective temperatures of supergiant stars determined by other authors (ordinates) against the $T^f_{\rm eff}$ estimates obtained in the present work (abscissa). The error bars correspond to temperatures inside the ellipse taken from Crowther et al. (2006) (vertical) and in the present work (horizontal). The square with a downward error bar indicates the systematic average shift that the McErlean et al. (1999) data might have.

T_{eff} (BCD) vs photometric determinations

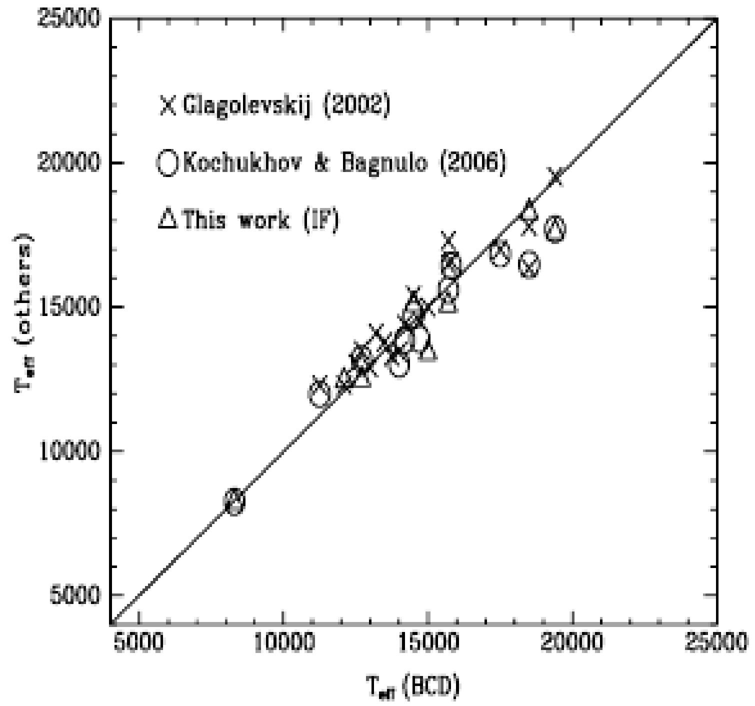

Fig. 1. Comparison of the effective temperatures derived from the BCD system with those obtained photometrically by Glagolevskij (2002), Kochukhov & Bagnulo (2006) and in this work with the integrated flux method.

Aidelman et al (2012) A&A 544, 64

log L_*/L_o (BCD) vs photometry

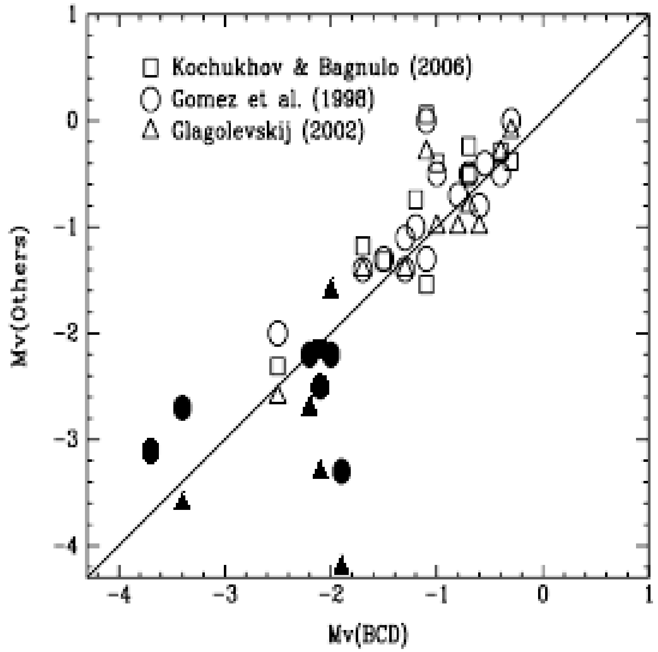

Fig. 2. Comparison of the visual absolute magnitudes derived from the BCD system with those derived by Gómez et al. (1998), Glagolevskij (2002) and Kochukhov & Bagnulo (2006). He-weak stars are represented by open symbols and He-strong stars by filled symbols.

distance is needed

Comparison of log g (BCD) vs evolutionary models

M_{bol} and T_{eff} are used with the evolutionary models to derive R* and M*

This allows us to obtain log g_{evol}

M* < 12 Mo and R* < 12 Ro   log g_{evol} > log g_{atm}

M* > 20 Mo and R* > 40 Ro   log g_{evol} < log g_{atm}

The mass discrepancy problem

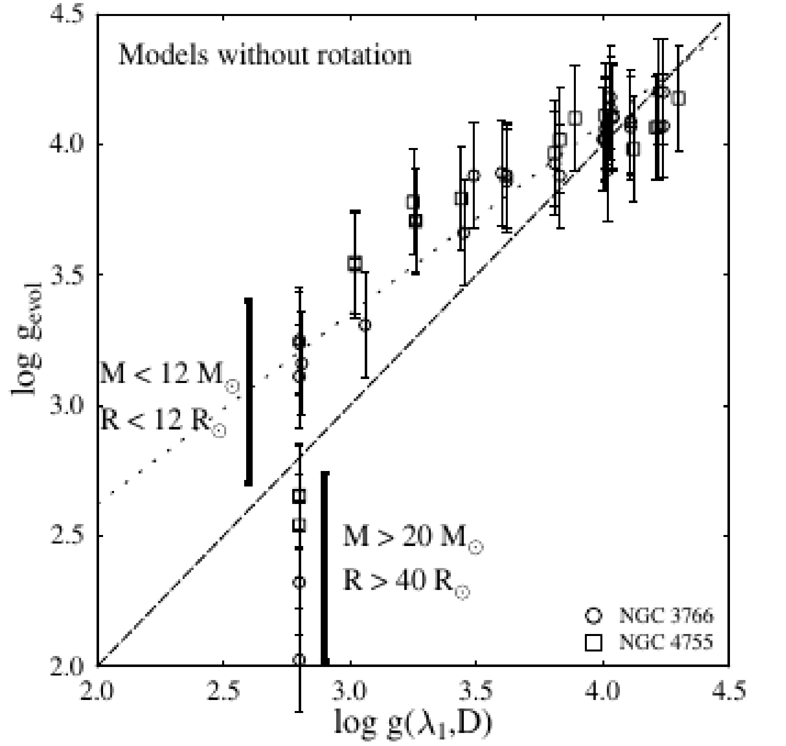

Fig. 13. Estimated log g_{evol} parameters with models of stellar evolution against log $g(\lambda_1, D)$ obtained with the BCD calibrations. As in Fig. 12, circles denote stars in NGC 3766, while squares denote stars in NGC 4755. We also indicate the marked stellar masses and radii for which log g_{evol} > log $g(\lambda_1, D)$ and those where log g_{evol} < log $g(\lambda_1, D)$. The evolutionary models used to infer stellar masses are those by Ekström et al. (2012) without rotation.

Aidelman et al (2012) A&A 544, 64

New results

Boller & Chivens Spectrographs

Spectral range 3500 Å y 5000 Å.
R=1000 -2000

Tartu Observatory, Estonia

Laboratório Nacional de Astrofísica, Brazópolis, Brazil

Complejo Astronómico El Leoncito (CASLEO), San Juan, Argentina

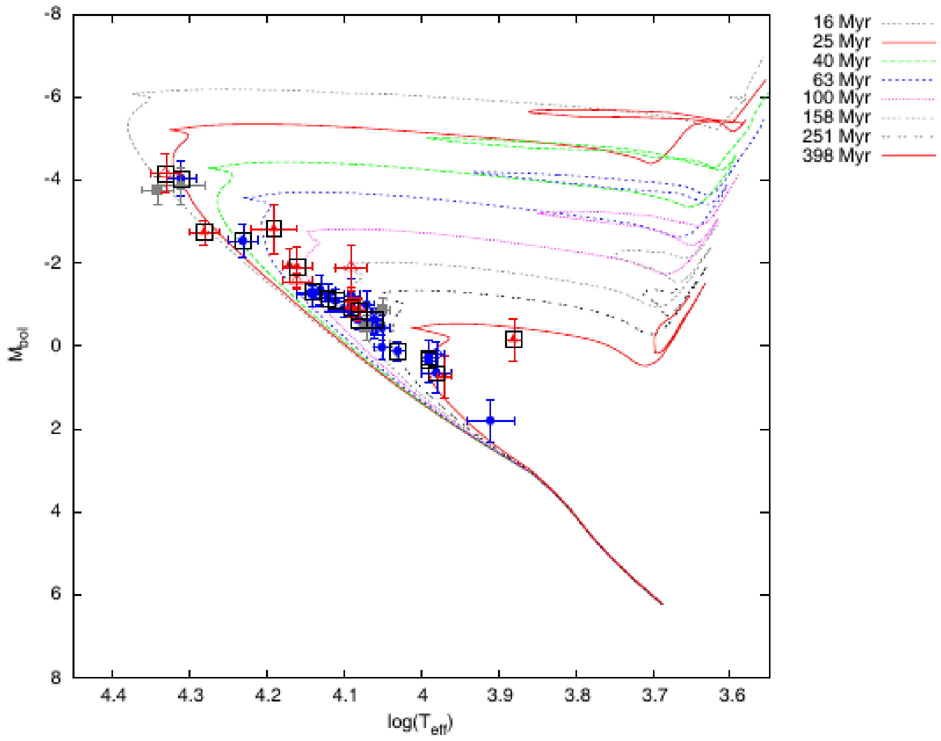

Fig. 6. NGC 3114: HR diagram. The isochrone curves are given by Ekström et al. (2012). Probable members of the clusters are denoted in • (blue) symbols, *pnm* in ⊙ (blue), and non-members (nm) in ■ (grey). Be star cluster members are indicated in ▲ (red) and Be *pnm* in △ (red). The stars denoted in □ symbols have a negative colour gradient excess.

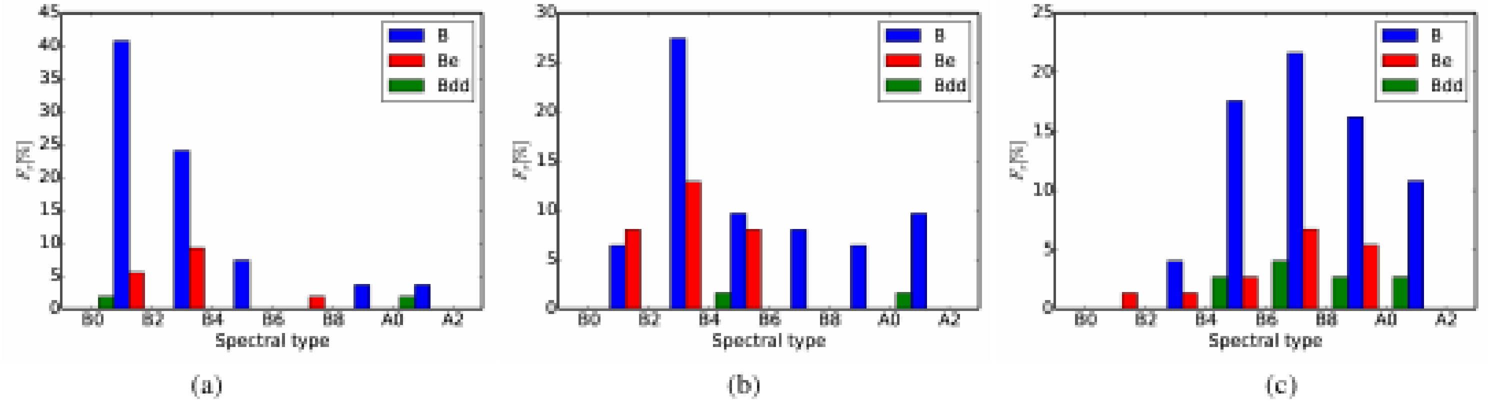

Fig. 15. Number and frequency of stars with and without circumstellar envelopes per spectral subtype in open clusters with different ages: *a*) between 3 Myr and 10 Myr, *b*) between 10 Myr and 40 Myr, and *c*) older than 40 Myr. The plots show a clear trend of the appearance of the Be phenomenon with age.

B supergiants

To search for stellar disks
Second Balmer discontinuity

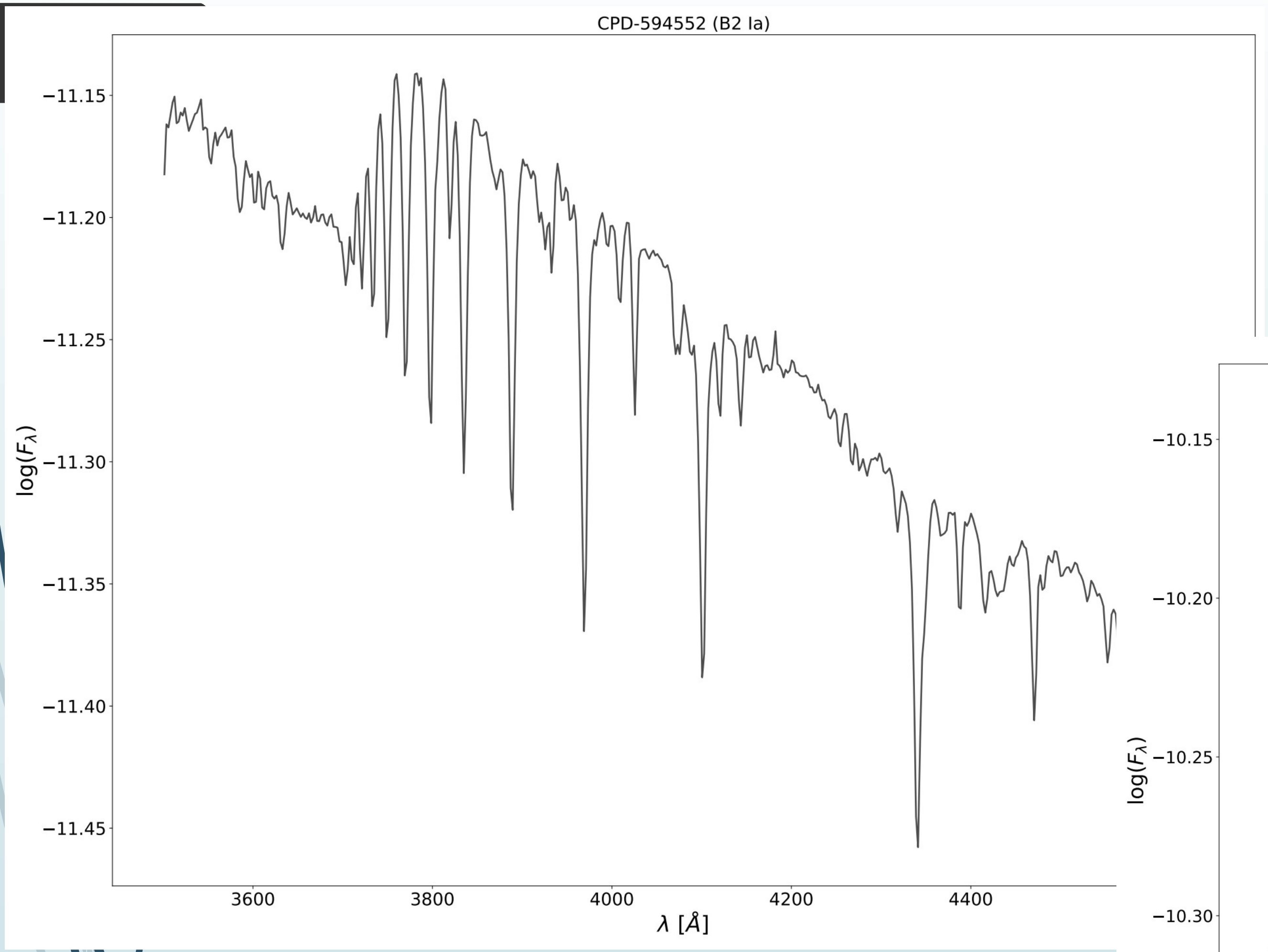

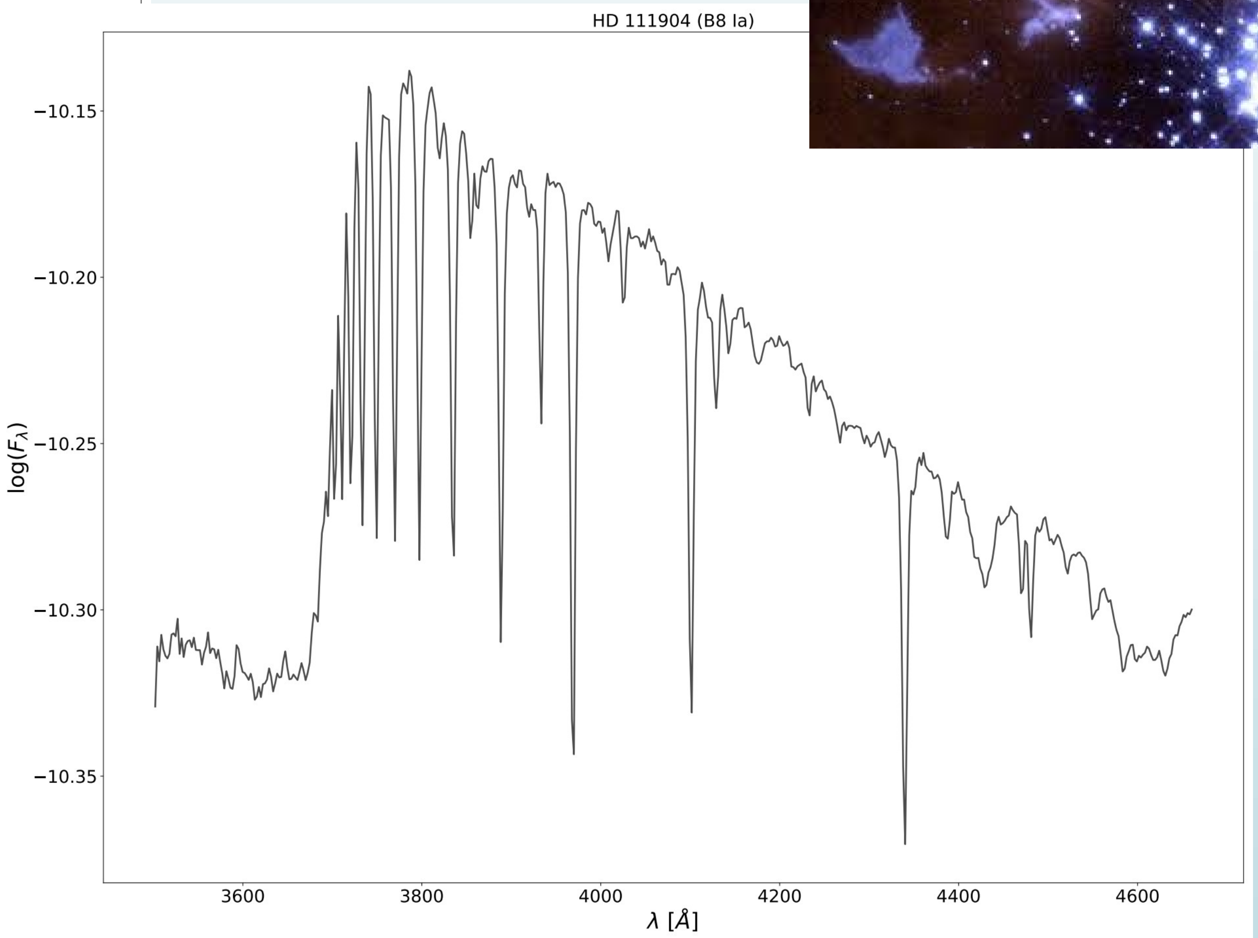

For classification purposes and derive stellar parameters

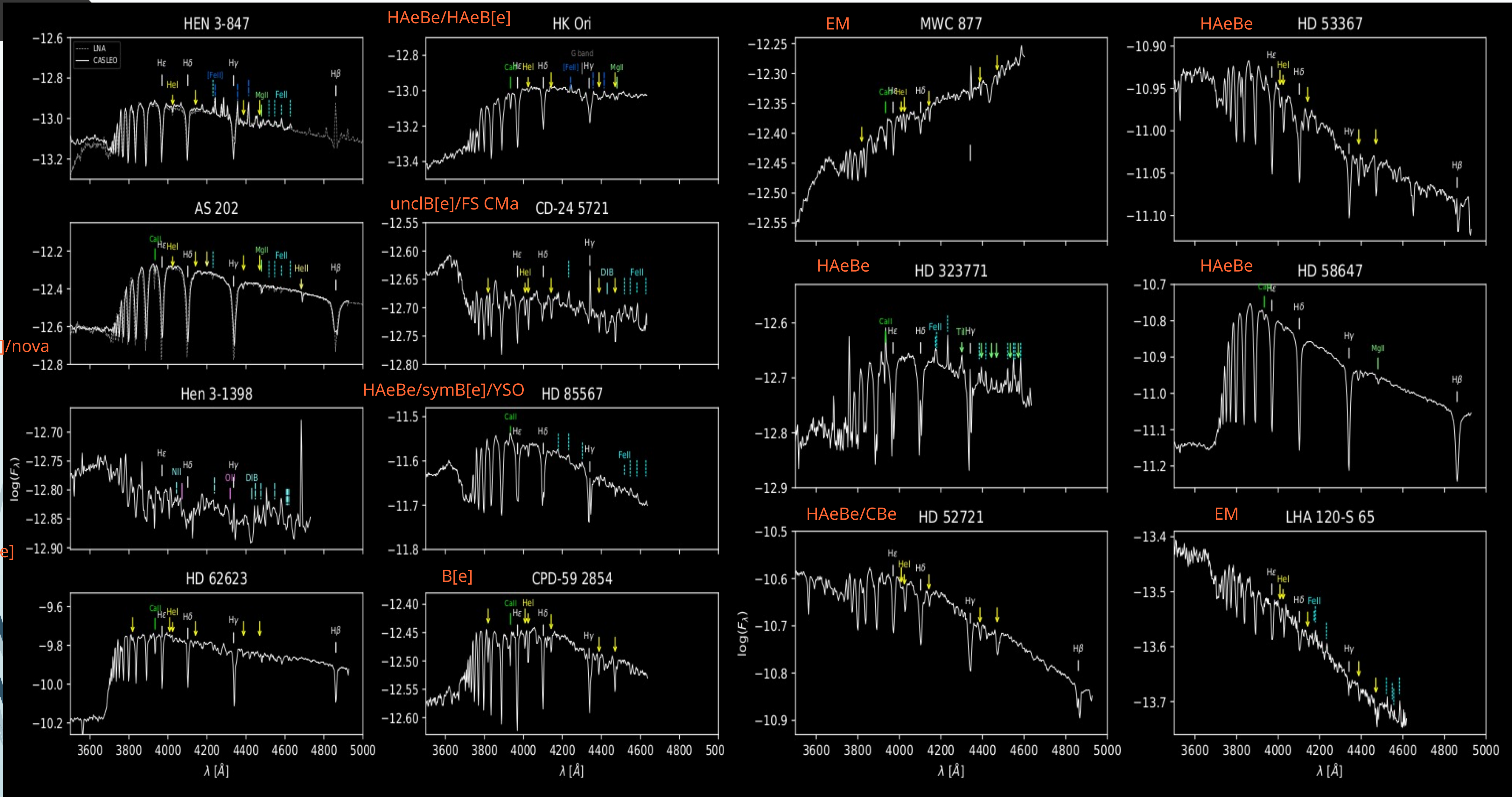

HAeBe/B[e]/nova

sgA[e]/sgB[e]

Supergigantes B[e]

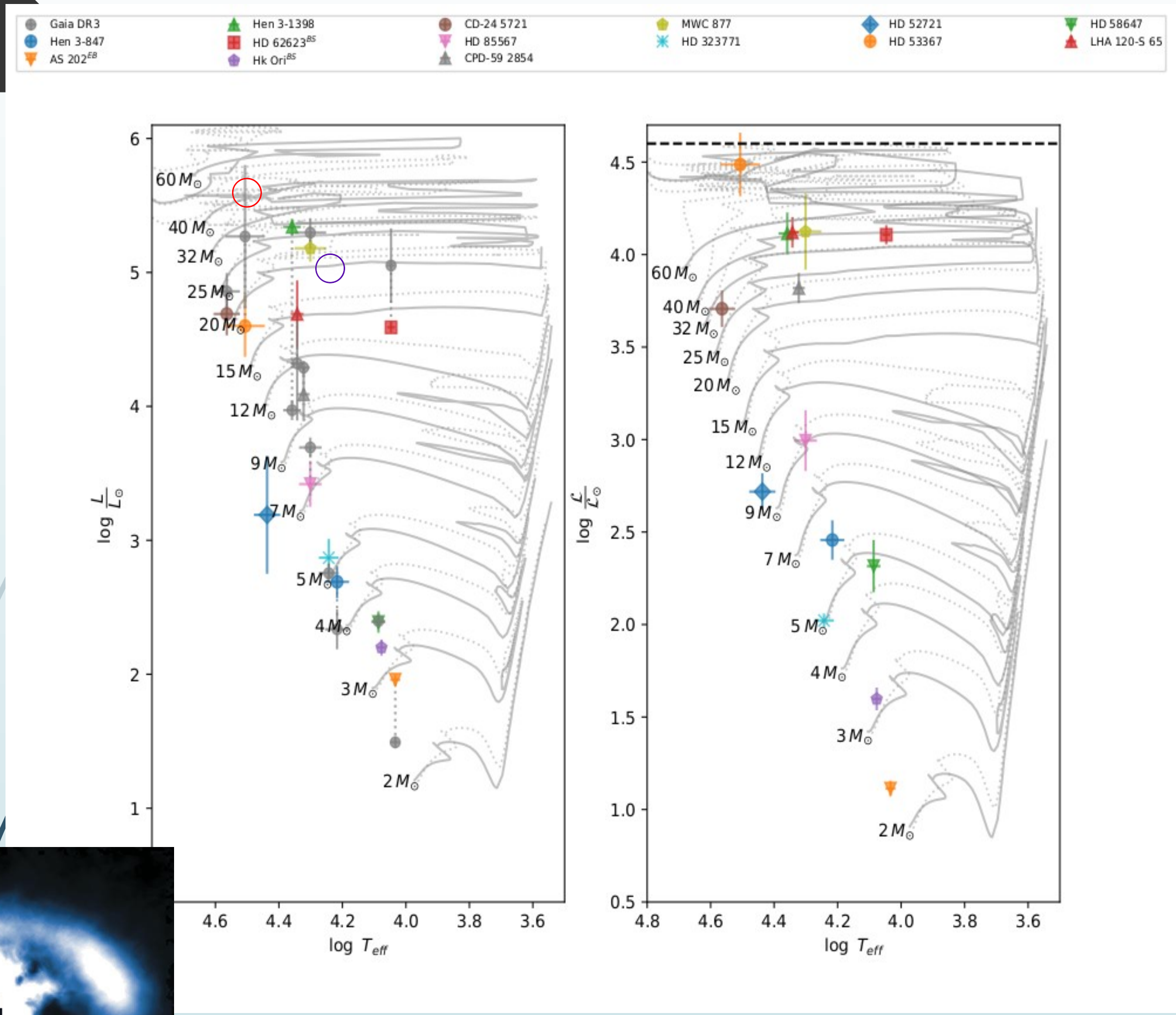

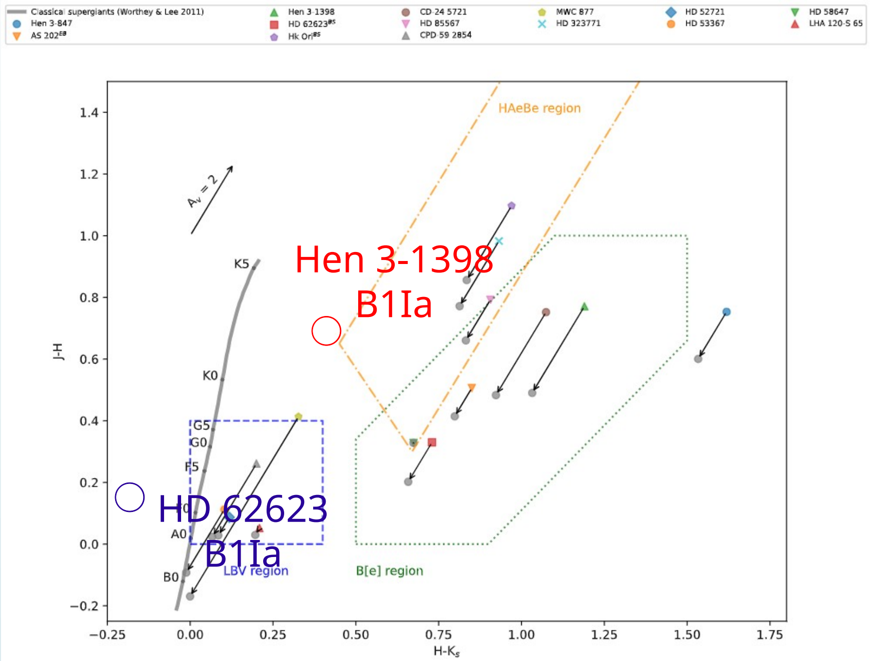

Cochetti et al. (2020), Kraus (2019), Oksala et al. (2013).

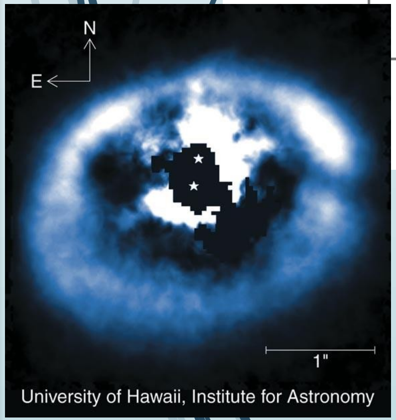

Créditos de Imagen: Observatorio GEMINI,
Daniel Potter

Herbig Ae/Be

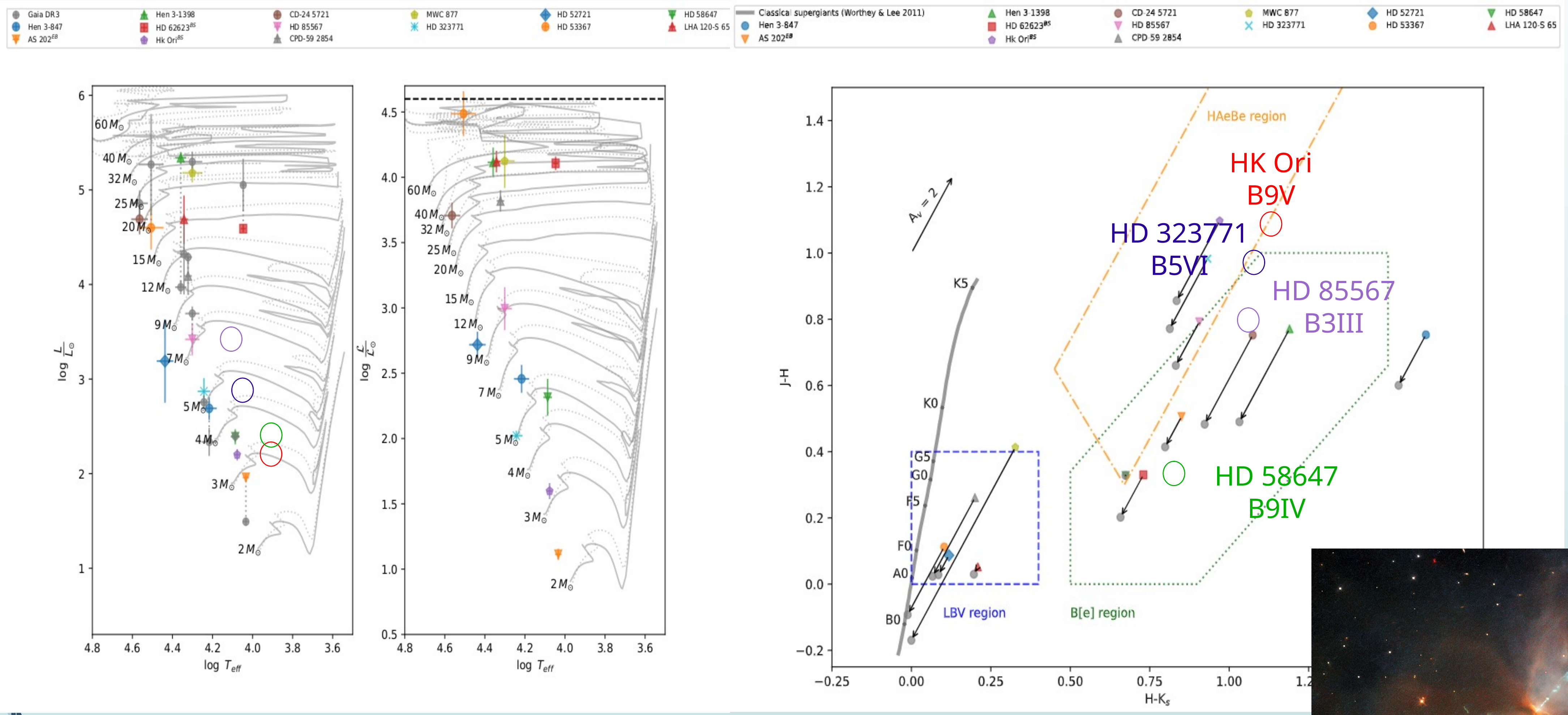

Gaia DR3
Hen 3-847
AS 202
Hen 3-1398
HD 62623
Hk Ori
CD-24 5721
HD 85567
CPD-59 2854
MWC 877
HD 323771
HD 52721
HD 53367
HD 58647
LHA 120-S 65
Classical supergiants (Worthey & Lee 2011)
log Teff
HAeBe region
LBV region
B[e] region
HK Ori
B9V
HD 323771
B5VI
HD 85567
B3III
HD 58647
B9IV
J-H
H-Ks

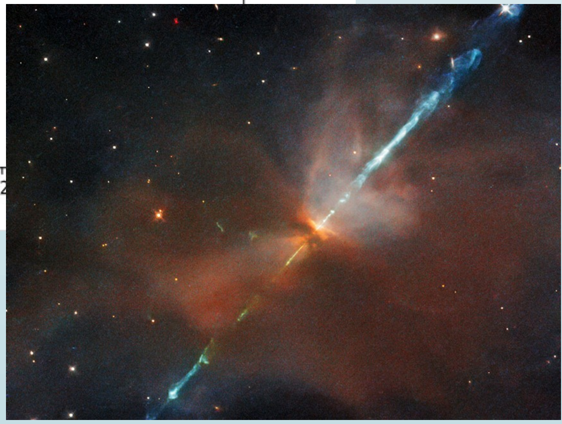

To study the temperature law across the surface

The binary system Algol (β Per). We acquired 22517 low-resolution spectra between September 2015 and February 2016 using the 1.5-m telescope AZT-12 of the Tartu Observatory (Folsom et al. 2022). Time-sequenced spectra were averaged over 5-minute intervals, reducing the observed sample to 856 spectra.

The BCD spectral classification allows to give a detail description of the temperature around the orbits

A limb darkening effect is seen over the stellar surface of the hot companion

Cidale, Aret, et al 2024, in preparation.

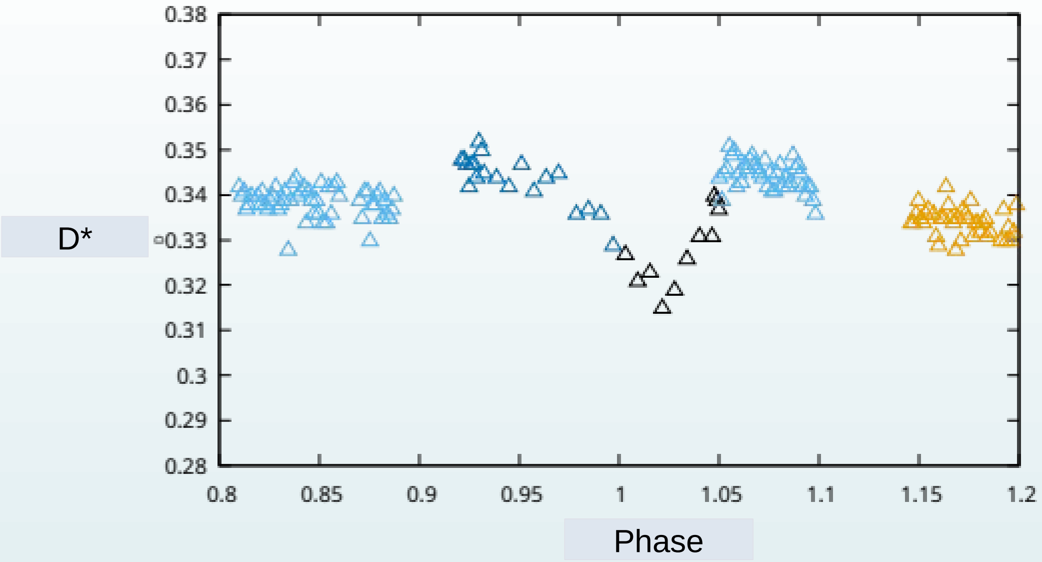

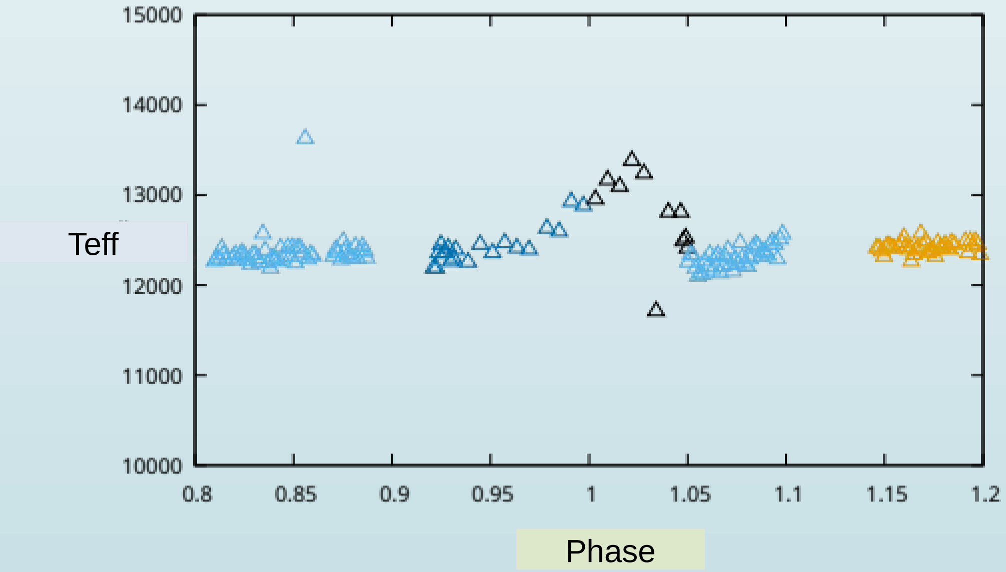

Preliminary results

Massive stars with stellar winds

Diagnostic lines

The T_{eff} is obtained from the ionization balance; e.g.: **Si II/Si III/Si IV**
He I/He II

- Uncertainties
  Teff of 300–500 K
  the Si ionisation balance
  and 1000 K for the He lines.
- Fitting procedure: “by eye”

Earlean et al. 1999
Urbaneja et al. 2005
Crowther et al 2006
Lefever et al. 2007
Searle et al. 2008
Markova & Puls 2008
Haucke et al., 2018, A&A 614, A91
Weßmayer et al., 2022, A&A, 668, A92

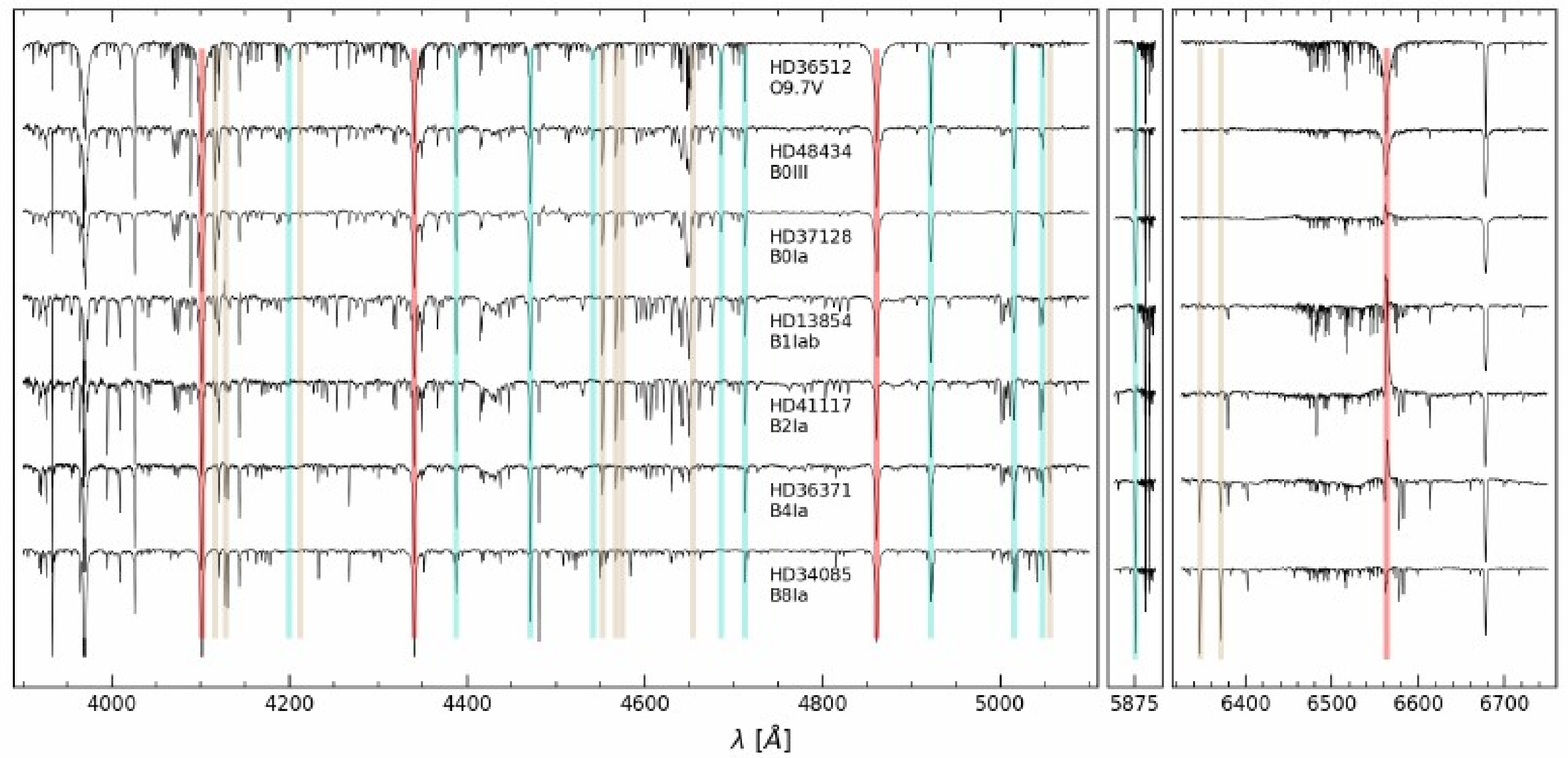

Fig. 1. Some illustrative examples of spectra used in this work, ordered by spectral type. Three different spectral windows depict the wavelength ranges in which the main diagnostic lines used to obtain estimates of the spectroscopic parameters are located. Vertical colored red, cyan, and brown bars indicate the corresponding H I, He I-II, and Si II-III-IV lines, respectively (see Sect. 3.2.3 for further details).

Burgos et al. 2024

Continuum Vs Spectral lines

The result could be different because the forming regions are different

Spectral lines form in the **upper** photosphere

The **continuum** form in the **lower** photosphere

log g (gravity) from **spectral lines** or the **Balmer jump**

Well-known NLTE wind codes

Mihalas, Kunasz, and Hummer (1975) presented a method for solving the line-formation problem using full comoving-frame formulation of the radiative-transfer equation for the case of spherically symmetric atmospheres expanding with arbitrarily large velocities. It initiated the development of numerical modeling methods and codes.

Hauschildt (1992) – fast method for the solution of the radiative transfer equation in rapidly moving spherical media, based on an approximate Λ-operator iteration

FASTWIND

Santolaya-Rey et al. (1997)

CMFGEN (and its predecessor)

Hillier (1987, 1990)
Hillier & Miller (1998)

WM-BASIC

Pauldrach, Puls, Kudritzki (1986)
Pauldrach et al. (2001)

PoWR

Hamann, Shmutz (1987),
Hamann et al. (1993)
Gräfener et al. (2002), Hartmann &Gräfener (2004)

PHOENIX

Hauschildt (1992)

log g, μ and micro (5-10 km s^{-1}), and macro (15-25 km s^{-1}) velocities

- Line spectral models
- The surface gravity (log g) is mainly defined by Hγ and Hδ lines.

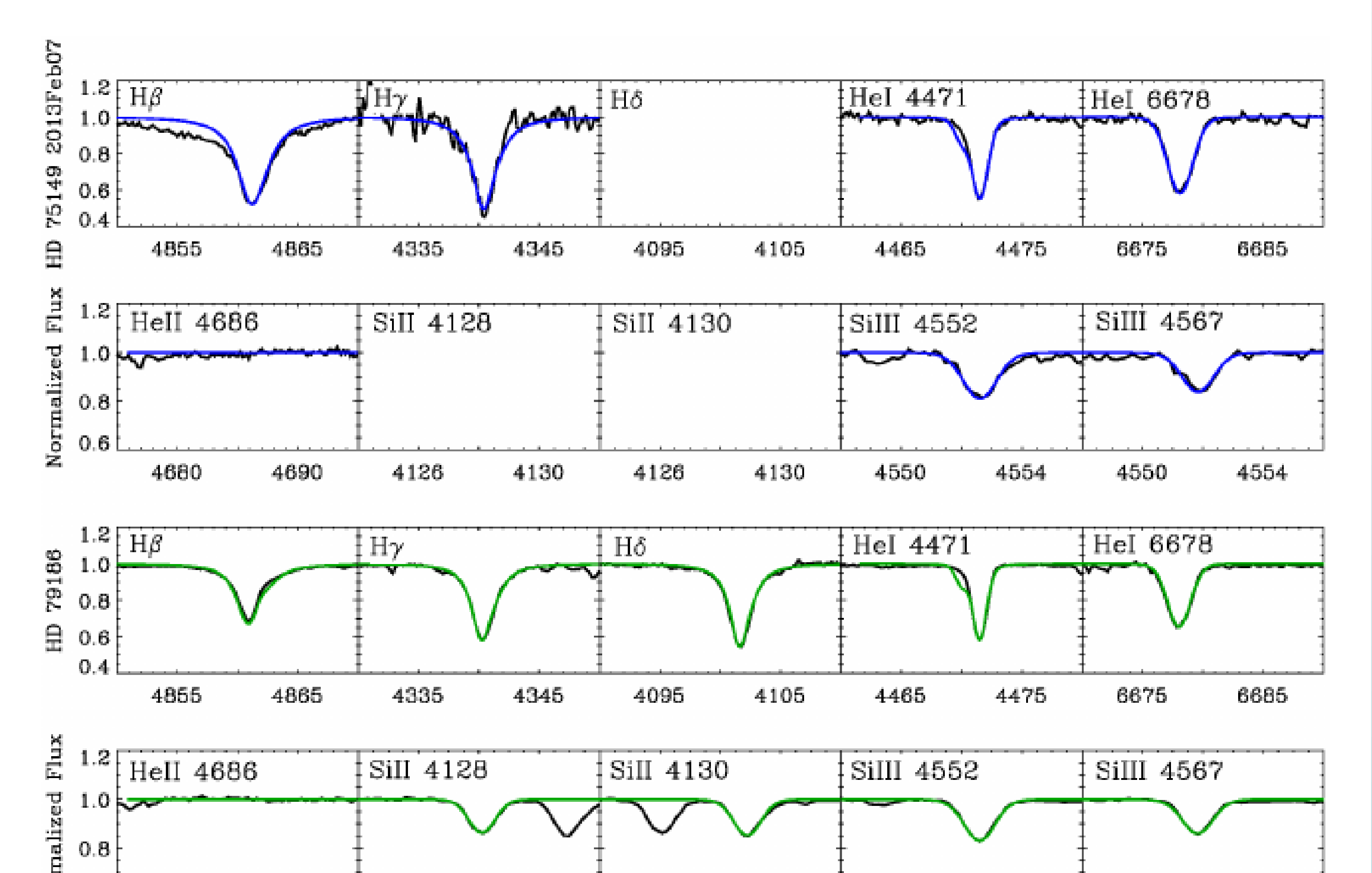

Haucke et al. (2018), A&A 614, A91

Analysis for 527 stars with O9 – B5 collected from IACOB database.

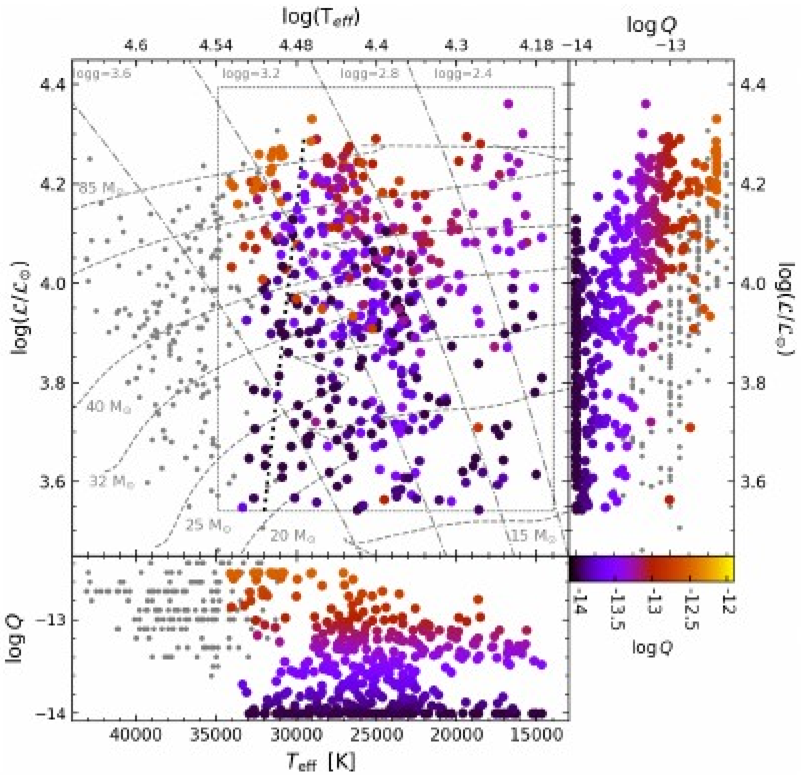

Fig. 14. sHR diagram of the stars in the sample color-coded by the wind-strength parameter. The bottom and right sub-panels in each panel show this quantity against $T_{\rm eff}$ and $\log \mathcal{L}$, respectively. Cases in which $\log Q$ is degenerate are excluded (see Sect. 4.1). All panels include 191 O-type stars from Hol18-22 indicated with gray circles. Evolutionary tracks are the same as in Fig. 7.

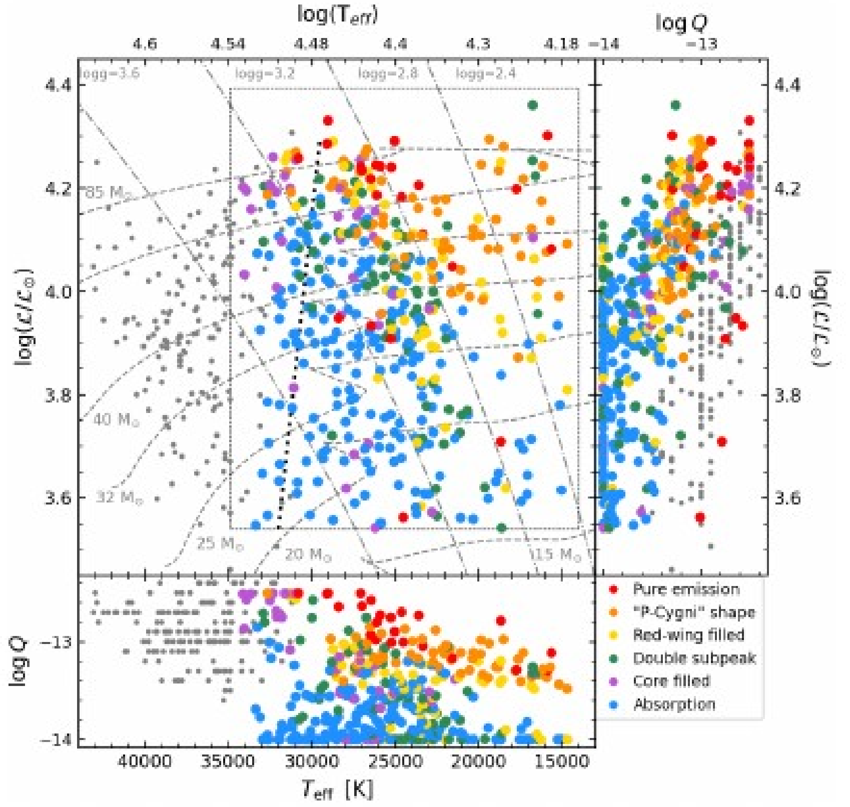

Fig. 15. Same as Fig. 14 but color-code representing the different shapes of the Hα line as classified in de Burgos et al. (2023, see also labels within the bottom right inset).

The atmospheric parameters were obtained using FASTWIND synthetic spectra in combination with a Markov chain Monte Carlo Method.

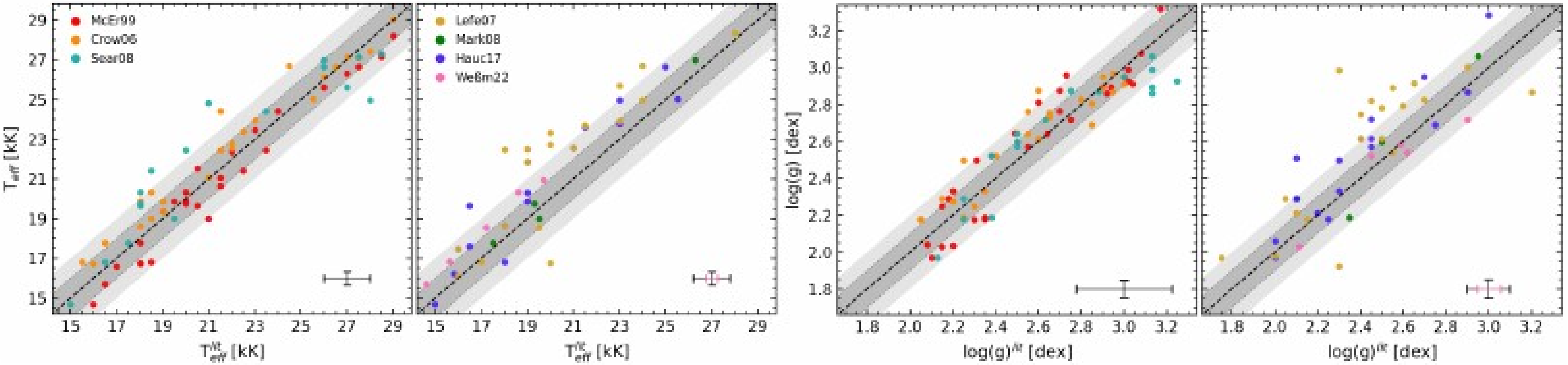

Fig. 5. Comparison of the results of the $T_{\rm eff}$ and log g with previous studies in the literature. Acronyms follow those in Table 4. The error bars in the bottom right corners indicate the average uncertainty from our analysis (vertical axis) or from the literature (horizontal axis) except those from Weßmayer et al. (2022) for which a separate error bar in pink has been included. The two shaded areas indicate a difference in $T_{\rm eff}$ and log g of 1000 K and 0.1 dex, and 2000 K and 0.2 dex, respectively. The diagonal black line indicates the 1-to-1 agreement.

Linear relationship for B supergiants

log Teff-log g

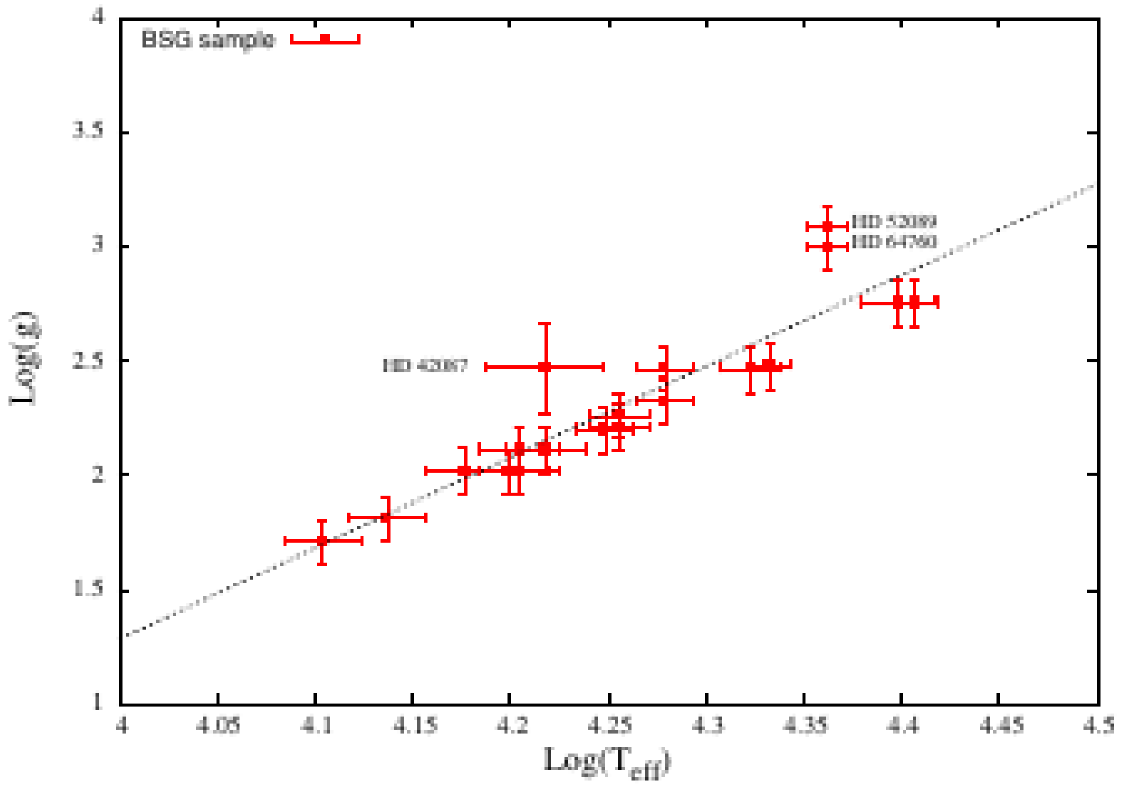

Fig. 7. Linear relation (log $T_{\rm eff}$–log $g_{\rm cor}$) of our sample of B Galactic supergiants (dashed line). The surface gravity was corrected by the centrifugal acceleration.

Haucke et al. (2018), A&A 614, A91

Wind Parameters

Massive stars have non-negligible stellar winds with mass-loss rates in the order of 10^{-8} – 10^{-7} $M_\odot$ yr^{-1}
Once all the stellar parameters are obatined we have a photospheric model which is a boundary condition to compute a wind model

- A velocity law for the wind

a hydrodynamical solution

a β-law

- A temperature law for the wind (Radiative equilibrium – isothermal winds)
- Mass-loss rate $Q = \dot{M}/(R_\star V_\infty)^{1.5}$
- Q, the wind-strength parameter (log Q), is a combination of mass-loss rate, wind terminal velocity and stellar radius (Puls et al. 1996, 2005).

$$v = v_\infty(1 - \frac{r_o}{r})^\beta$$

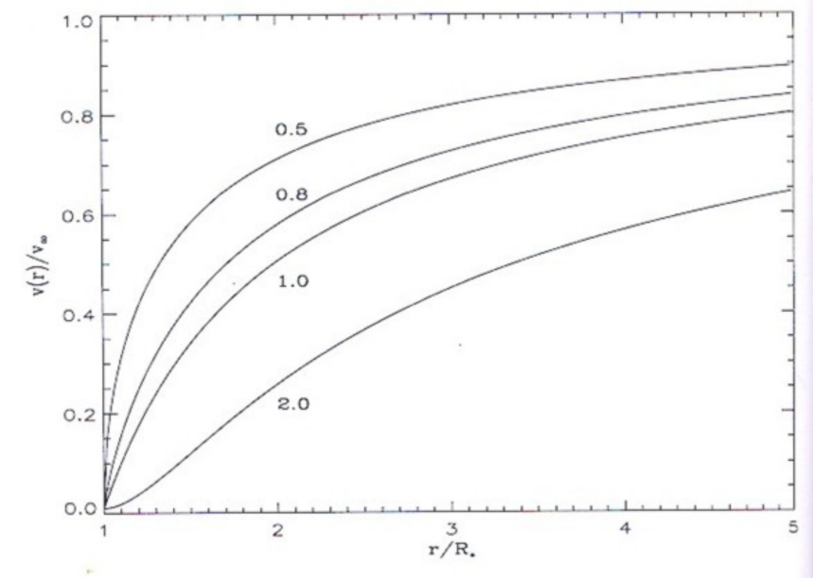

A&A 614, A91 (2018)

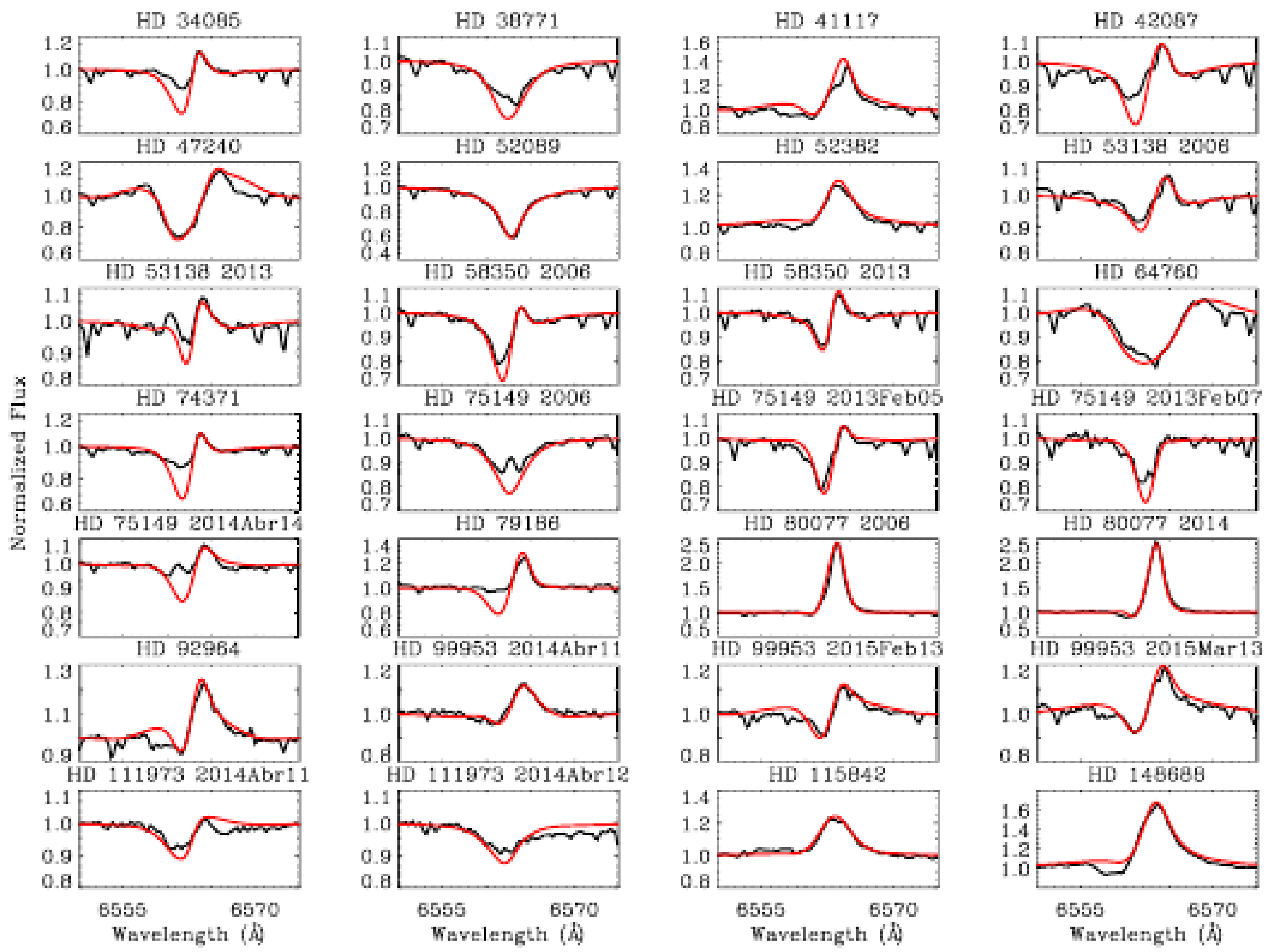

Fig. 1. Hα line and the best-fitting synthetic model. For HD 53138, HD 58350, HD 75149, HD 80077, HD 99953, and HD 111973 more than one plot are shown due to multi-epoch observations.

The shape and strength of the Hα profile can provide constraints simultaneously on the wind acceleration β and the wind-strength parameter Q.

Mass-loss Recipes

Radiative mass-loss rate by Vink et al. (2000)

$$\log \dot{M} = -6.697(\pm 0.061) + 2.194(\pm 0.021)\log(L_*/10^5) - 1.313(\pm 0.046)\log(M_*/30) - 1.226(\pm 0.037)\log\left(\frac{v_\infty/v_{\rm esc}}{2}\right) + 0.933(\pm 0.064)\log(T_{\rm eff}/40000) - 10.92(\pm 0.90)\{\log(T_{\rm eff}/40000)\}^2$$

for $27\,500 < T_{eff} \leq 50\,000$K

!!! These ratios are used in Geneva evolutionary models

$$\log \dot{M} = -6.688(\pm 0.080) + 2.210(\pm 0.031)\log(L_*/10^5) - 1.339(\pm 0.068)\log(M_*/30) - 1.601(\pm 0.055)\log\left(\frac{v_\infty/v_{\rm esc}}{2}\right) + 1.07(\pm 0.10)\log(T_{\rm eff}/20000)$$

for $12\,500 < T_{eff} \leq 22\,500$K

Mass-loss Recipes

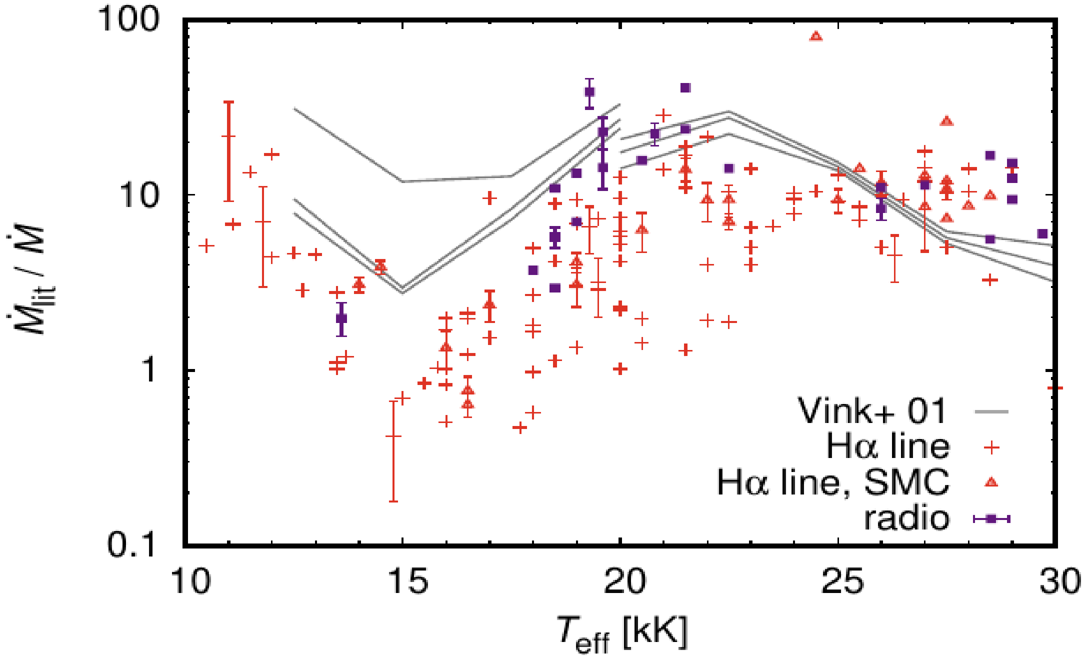

Krtička et al. 2021

$$\log\left(\frac{\dot{M}}{1M_\odot \mathrm{yr}^{-1}}\right) = a + b\log\left(\frac{L_*}{10^6 L_\odot}\right) - a\log\left\{\exp\left(-\frac{(T-T_1)^2}{\Delta T_1^2}\right) + c\exp\left(-\frac{(T-T_1)^2}{\Delta T_1^2}\right)\right\}$$

Björklund et al. 2022

$$\log \dot{M} = -5.52 + 2.39\log\left(\frac{L_*}{10^6 L_\odot}\right) - 1.48\log\left(\frac{M_*}{45M_\odot}\right) + 2.12\log\left(\frac{T_{\rm eff}}{4500K}\right) + \left(0.75 - 1.87\log\left(\frac{T_{\rm eff}}{4500K}\right)\right)\log\left(\frac{Z_*}{Z_\odot}\right)$$

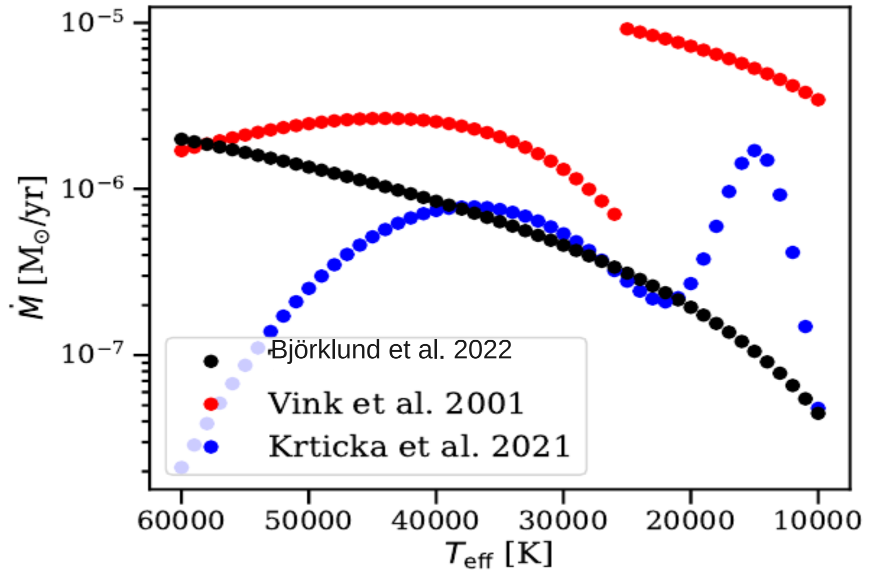

Cidale, L. S., et al.: A&A, 677, A176 (2023)

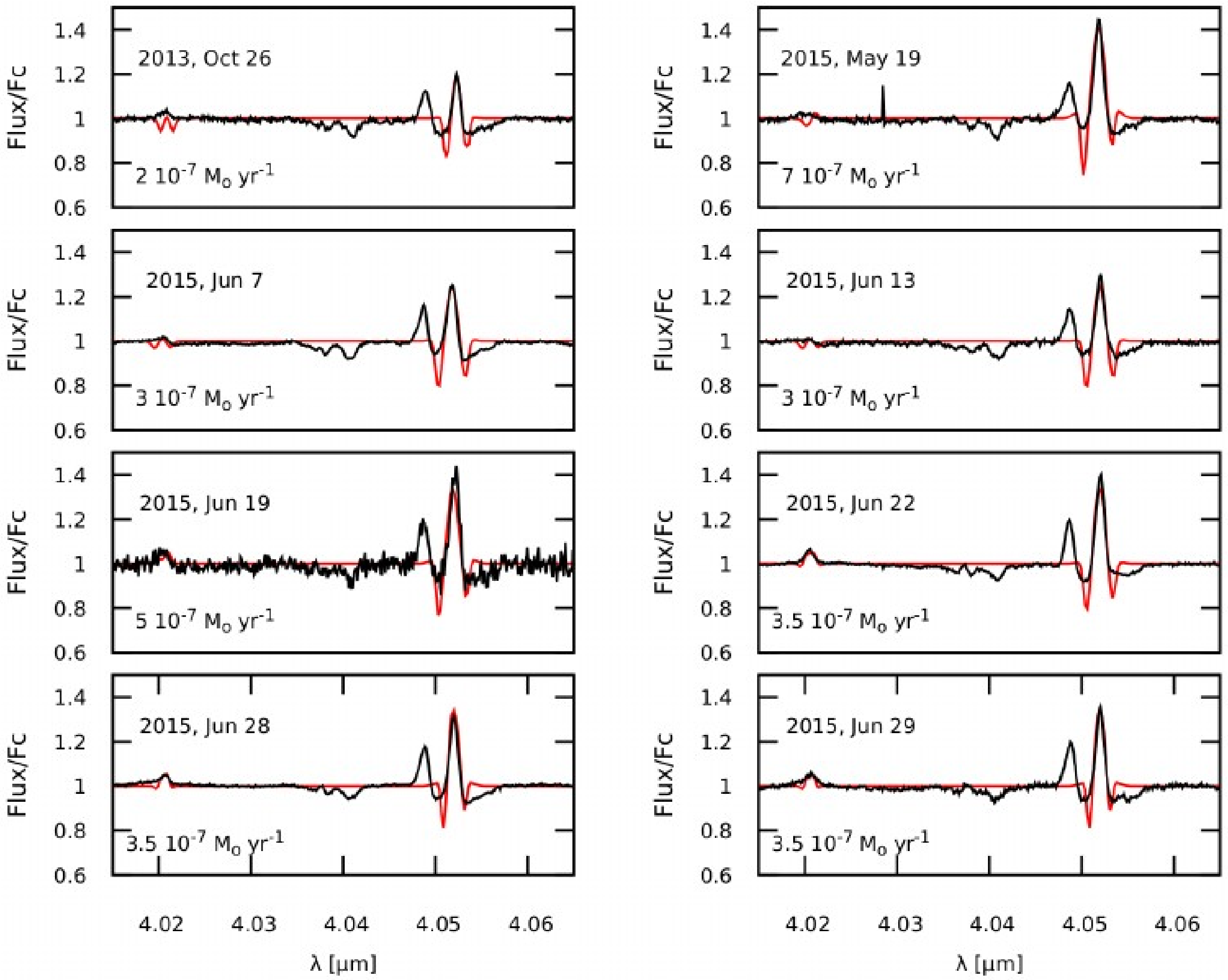

Fig. 8. Best-fitting models to the Brα and Hu_{14} emission observed in 2013 and 2015. Observations are traced in black, and models are in solid red lines. The mass-loss rate used to model the lines is indicated in each plot.

55 Cyg

Mass-loss variations of a factor of two in 22 days.

IR spectroscopy. Fittings to the Brα line.

Appel code (Mihalas & Kunasz (1998)

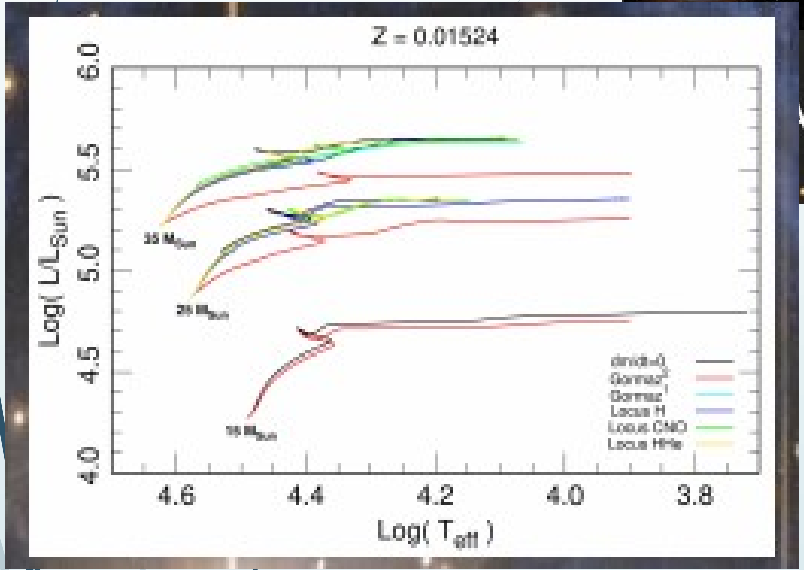

POEMS

Different recipes for the mass-loss rates of O and B stars

A. Panei[1,2], F. Figueroa-Tapia[3], M. Curé[3,4], I. Araya[5], L. S. Cidale[1,2], R. O. J. Venero[1,2], and A. C. Gormaz-Matamala[3,6,7]

Visit posters

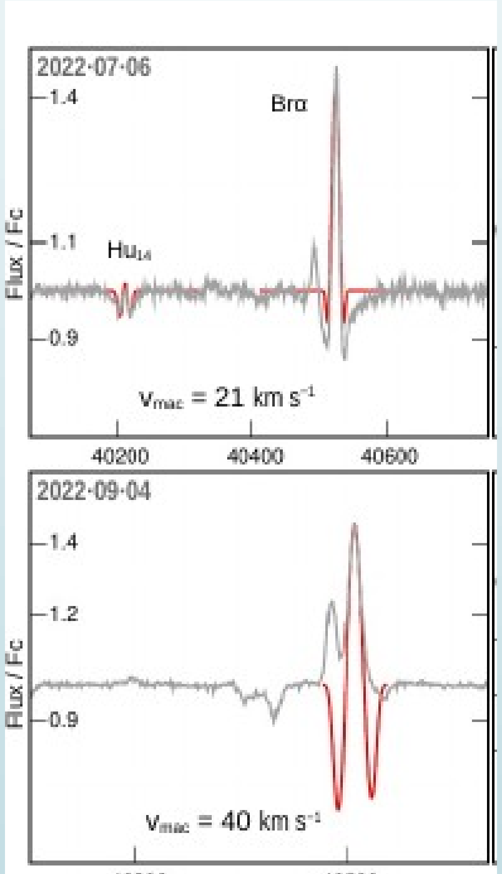

Stellar Wind Parameter Determination through Modeling IR Line Profiles in B-type Supergiants

L. V. Mercanti[1,2] · L. S. Cidale[1,2] · A. F. Torres[1,2] · M. L. Arias[1,2] · R. O. J. Venero[1,2] · O. Maryeva[3] · M. Kraus[3]

Are the models unique?

Fast Regime

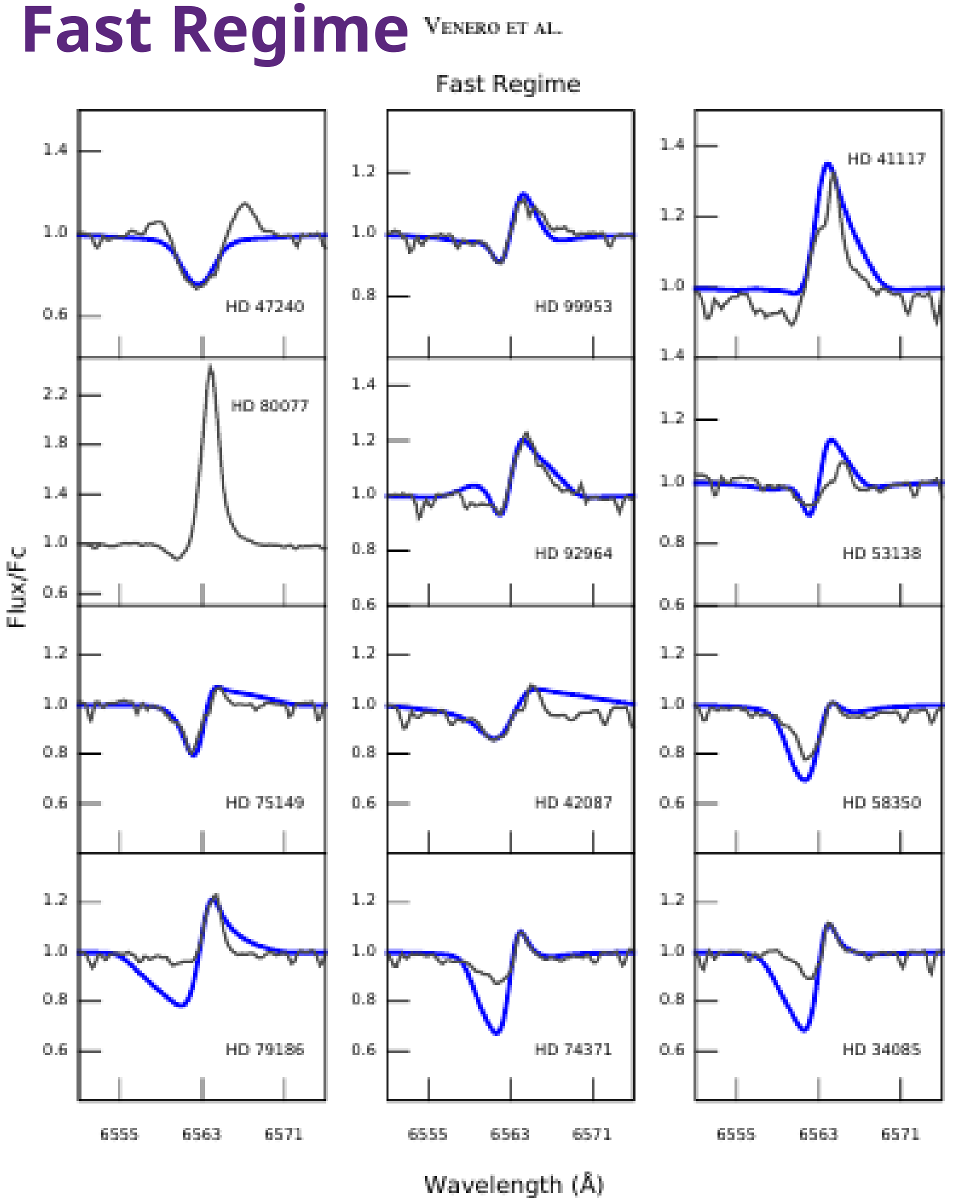

Slow Regime

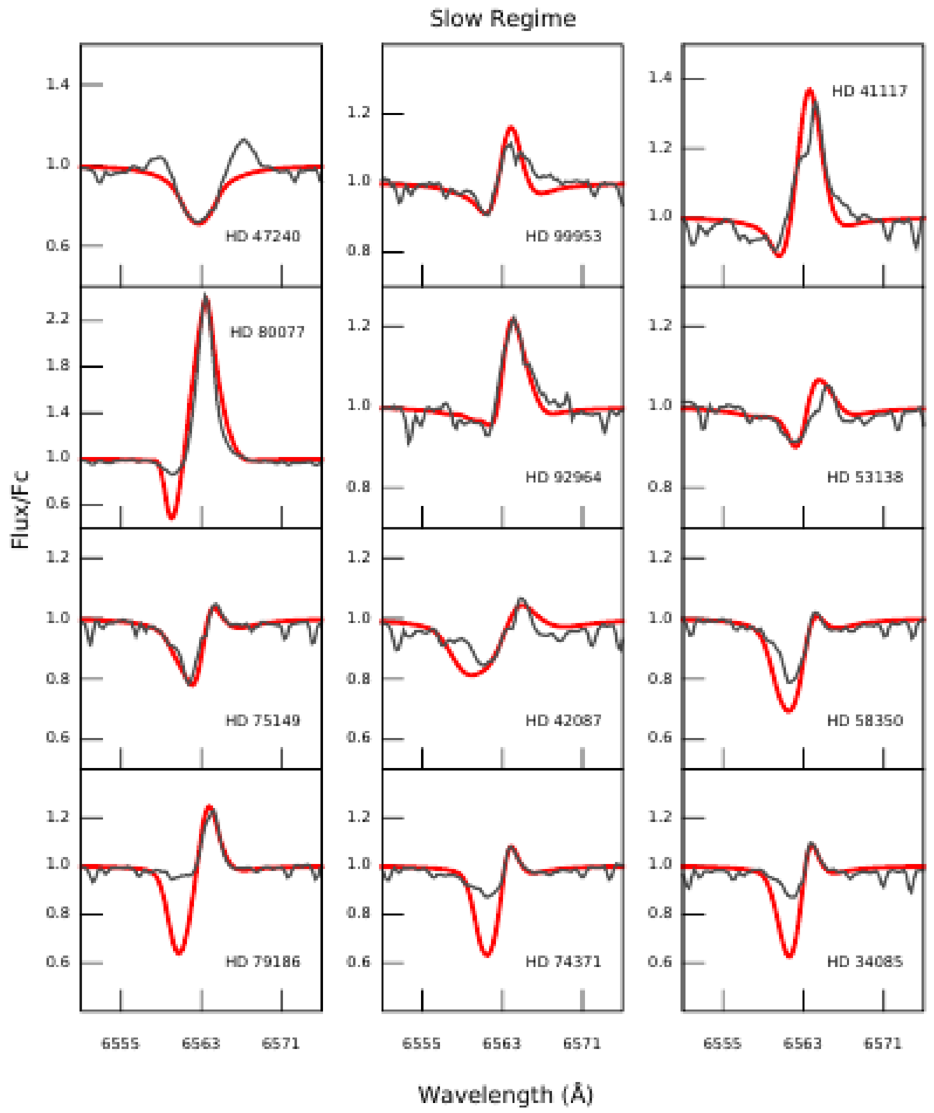

Determination of parameters of the environments

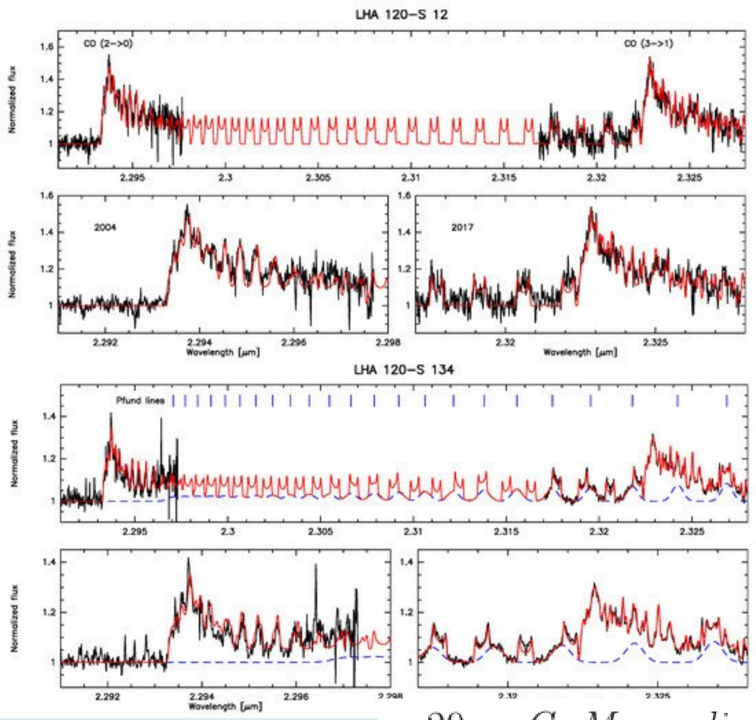

Kraus et al. 2023, Galaxies 11, 76

Emission molecular emission & forbidden lines

The post-main sequence evolution of massive stars lose a significant amount of mass that leads to molecular discs. Model with rings!

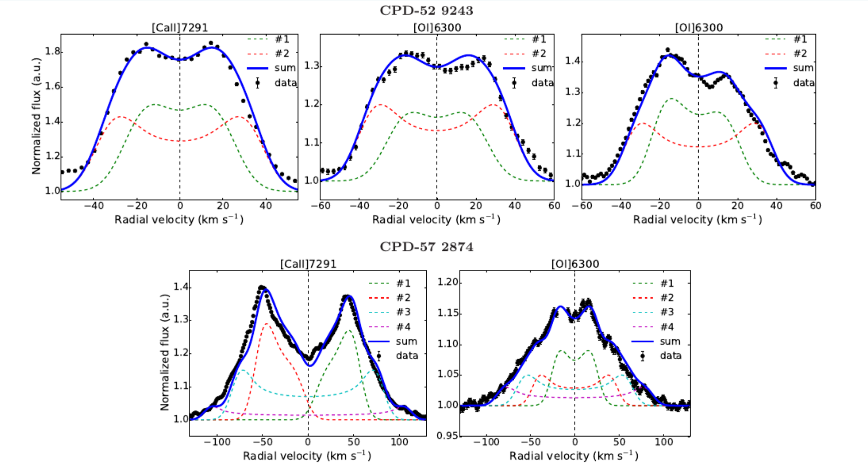

20 *G. Maravelias et al.*

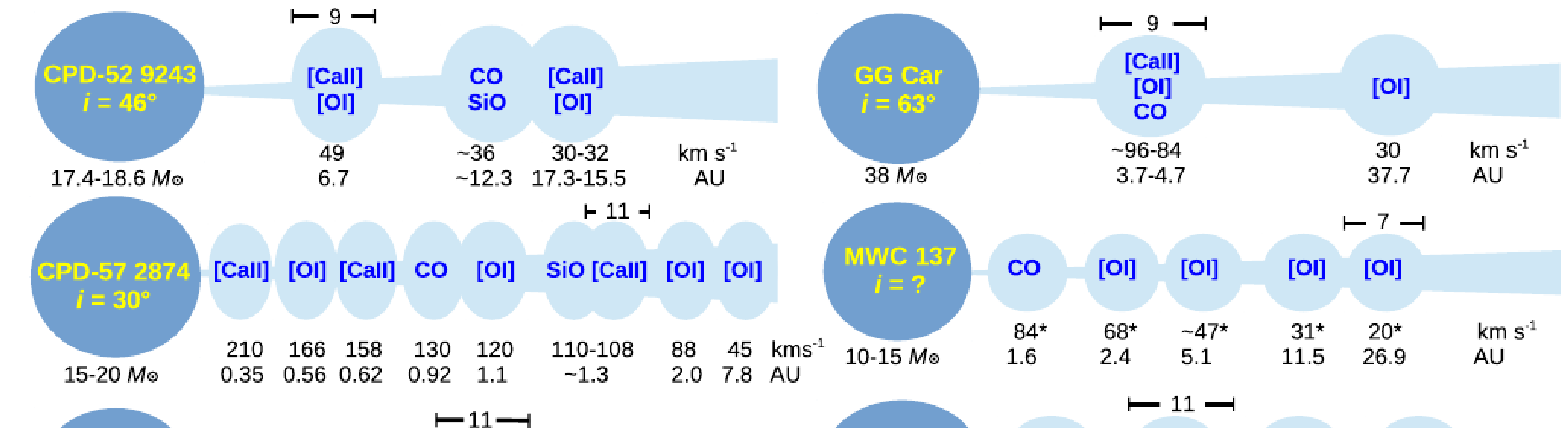

Maravelias et al., 2018

Final Remarks

- We describe the use of various methods to derive fundamental parameters.
- The combination of different methods is always positive, but it could provide values that are not self consistent.
- The BCD method has clear advantages and very well known limitation. We report supergiants with discs and variation of the temperature over the stellar disc.
- Investigations of the mass-loss and the circumstellar environment of evolved stars benefit from synergies of optical/infrared spectroscopy.
- Lack of unicity in the wind modelling.
- Mass loss variability and its effects on stellar evolution.

Thank you


International Conference
Physics of Extreme Massive Stars
24 – 28 June 2024
Rio de Janeiro, Brazil